

A computational formulation for constrained solid and liquid membranes considering isogeometric finite elements

Roger A. Sauer¹, Thang X. Duong, Callum J. Corbett

Aachen Institute for Advanced Study in Computational Engineering Science (AICES), RWTH Aachen University, Templergraben 55, 52056 Aachen, Germany

Published² in *Computer Methods in Applied Mechanics and Engineering*,

DOI: [10.1016/j.cma.2013.11.025](https://doi.org/10.1016/j.cma.2013.11.025)

Submitted on 17. October 2012, Revised on 11. November 2013, Accepted on 29. November 2013

Abstract

A geometrically exact membrane formulation is presented that is based on curvilinear coordinates and isogeometric finite elements, and is suitable for both solid and liquid membranes. The curvilinear coordinate system is used to describe both the theory and the finite element equations of the membrane. In the latter case this avoids the use of local cartesian coordinates at the element level. Consequently, no transformation of derivatives is required. The formulation considers a split of the in-plane and out-of-plane membrane contributions, which allows the construction of a stable formulation for liquid membranes with constant surface tension. The proposed membrane formulation is general, and accounts for dead and live loading, as well as enclosed volume, area, and contact constraints. The new formulation is illustrated by several challenging examples, considering linear and quadratic Lagrange elements, as well as isogeometric elements based on quadratic NURBS and cubic T-splines. It is seen that the isogeometric elements are much more accurate than standard Lagrange elements. The gain is especially large for the liquid membrane formulation since it depends explicitly on the surface curvature.

Keywords: contact constraints, curvilinear coordinates, isogeometric analysis, nonlinear finite element methods, follower loads, volume constraints.

1 Introduction

Membranes are computationally challenging structures. Their geometry can be complex, they may undergo large deformations, large rotations and large strains – and thereby behave highly nonlinear – and they are characterized by several physical instabilities: They are unstable in compression, unstable for out-of-plane loading (in the case of zero in-plane tension), unstable for pressure loading (in the case of rubber membranes) and unstable w.r.t. in-plane loading (in the case of liquid membranes). The aim of this paper is to formulate a general, 3D, geometrically exact and fully nonlinear computational membrane model that accounts for pressure loading as well as volume, area, and contact constraints and is suitable for both solid and liquid membranes. Our focus is on pure membranes, i.e. curved, surface structures that do not support in-plane compression, out-of-plane bending, and shear.³ Such a restricted focus is useful due to the

¹corresponding author, email: sauer@aices.rwth-aachen.de

²This pdf is the personal version of an article whose final publication is available at www.sciencedirect.com

³We note that in the literature, the term membrane is often also used for the special case of 2D plane-stress structures.

large range of membrane applications: they appear as inflatable and pressurized structures, like balloons, tubes and airbags; as fabrics, tents, canopies, parachutes, foils and sails; as water-filled membrane structures, like inflatable dams; as biological membranes, like blood vessels, cells, diaphragms, aneurysms and lung alveoli; as liquid droplets, menisci, bubbles, foams and sprays; as thin sheets and films – both liquid and solid – as atomistic membranes, like graphene sheets; as interacting membranes, e.g. adhering cells; and in the topic of form-finding and minimal surfaces.

Computational formulations for 3D, nonlinear membrane go back to the seminal work of Oden (Oden and Sato (1967), see also Oden (2006)). Since then, the field has been continuously advanced, among others by Fried (1982); Tang (1982); Roddeman et al. (1987); Contri and Schrefler (1988); Wriggers and Taylor (1990); Ibrahimbegovic and Gruttmann (1993); Haseganu and Steigmann (1994); Gosling and Lewis (1996); Muttin (1996); Wu et al. (1996); Bonet et al. (2000); Rumpel and Schweizerhof (2003); Stanuszek (2003); Weinberg and Neff (2008). Many of these works are concerned with the topic of wrinkling due to in-plane compression. Relevant to membranes is also the work on shells, since they typically contain membranes as special cases. Geometrically exact computational shell formulations go back to the work of Simo and Fox (1989) and Simo et al. (1990). A review of the topic can be found in Bischoff et al. (2004). Recently, shell formulations have been proposed in the context of isogeometric analysis (Kiendl et al., 2009; Benson et al., 2011; Nguyen-Thanh et al., 2011). The fact that solid membranes can be extracted out of shell theory does not imply that this will work robustly in computations, which is why computational membrane formulations are important by themselves. Computational formulations based on curvilinear coordinates have been considered rigorously, both for membranes (Ambroziak and Klosowski, 2006) and shells (Arciniega and Reddy, 2007). Another recent development are rotation-free shell formulations, as they have been considered by Flores and Estrada (2007); Linhard et al. (2007); Dung and Wells (2008) and recently Benson et al. (2011); Nguyen-Thanh et al. (2011) for isogeometric analysis. Isogeometric formulations allow the formulation of C^1 -continuous surface formulations that are advantageous for flow simulations (Kiendl et al., 2010) and sliding contact (De Lorenzis et al., 2011; Temizer et al., 2012); in this regard see also Sauer (2011, 2013a) for Hermite-based, C^1 -continuous contact surfaces. Relevant to membranes is also the topic of live pressure loading (Bufler, 1984; Schweizerhof and Ramm, 1984). Membranes are also an interesting subject in shape optimization (Bletzinger et al., 2005; Manh et al., 2011).

This paper is concerned with several modeling aspects that are not considered in the computational formulations mentioned above. The most important of these are the inclusion of liquid membranes and the inclusion of several corresponding constraints and properties (like contact angles) into our formulation. We are also motivated by the provision of a novel pure membrane formulation for solids. This formulation is based on the theoretical framework of Steigmann (1999), which has not yet been extended to a computational formulation. The presented formulation also contains several further merits and novelties: It allows for a split between in-plane and out-of-plane contributions, which is used to construct a new formulation for liquid membranes. It admits arbitrary elastic material models for solid and liquid membranes. In the case of liquid membranes, the formulation is capable of capturing the complex mechanical behavior at liquid interfaces that is a consequence of different interface energies and the surface topology.⁴ The formulation constitutes an explicit formulation of the liquid surface that is more general than the explicit finite element formulation of Brown et al. (1980), and is an alternative to immersed boundary and phase-field methods, e.g. see Dong (2012) for a recent example. In distinction to the work of Javili and Steinmann (2010), which extends surface energies to bulk

⁴The current formulation is restricted to quasi-static, continuum mechanical systems. Dynamical, atomistic and non-mechanical behavior are outside our present scope.

systems, our formulation considers problems that are purely described by surface quantities.

Our formulation is based purely on displacement-based finite elements and can be used with any kind of such elements. It includes, in particular, isogeometric NURBS elements to capture the deforming surface geometry to high-accuracy, even for comparably coarse discretizations. It is straight forward to implement in an existing FE framework. It avoids the need to transform derivatives between configurations and avoids the use of local cartesian coordinate systems. Shell models are often formulated using local cartesian coordinate systems, as this allows using classical constitutive relations formulated in this manner (Wriggers, 2008). To our mind, there is no need for such a detour: The balance laws, kinematics, constitutive relations as well as the FE weak forms and corresponding FE arrays can all be formulated efficiently in the curvilinear coordinate system. The capabilities of the presented formulation are demonstrated by several challenging computational examples, considering pressure loading, inflation and contact.

The following section presents the theory of nonlinear membranes in the framework of curvilinear coordinates, considering pressure loading, volume, area and contact constraints. Sec. 3 proposes a straight-forward finite element implementation of the theory, and Sec. 4 presents several examples of solid and liquid membranes to illustrate the capabilities of the present formulation.

2 Nonlinear membranes

In this section, we summarize the theory of nonlinear membranes in the framework of curvilinear coordinates. The membrane kinematics, constitution and balance laws in strong and weak form are discussed, and various kinds of constraints are considered. Details on curvilinear coordinates can for example be found in Kreyszig (1991) and Steigmann (1999).

2.1 Surface description in curvilinear coordinates

The membrane surface, denoted \mathcal{S} , is fully characterized by the parametric description

$$\mathbf{x} = \mathbf{x}(\xi^1, \xi^2) . \quad (1)$$

This corresponds to a mapping of the point (ξ^1, ξ^2) in the parameter domain \mathcal{P} to the material point $\mathbf{x} \in \mathcal{S}$. In the following, Greek letters are used to denote the two indices 1 and 2. Summation is then implied on repeated indices. The tangent vectors to coordinate ξ^α at point $\mathbf{x} \in \mathcal{S}$ are given by

$$\mathbf{a}_\alpha = \frac{\partial \mathbf{x}}{\partial \xi^\alpha} , \quad \alpha = 1, 2 \quad (2)$$

The two vectors form a basis for the tangent plane of \mathcal{S} . In general, they are not orthonormal. This apparent drawback of the description is actually an advantage when it comes to the kinematical description. This turns out to be very straightforward, e.g. see Eq. (16). The basis at \mathbf{x} is characterized by the metric tensor, that has the co-variant components

$$a_{\alpha\beta} := \mathbf{a}_\alpha \cdot \mathbf{a}_\beta . \quad (3)$$

From the inversion

$$[a^{\alpha\beta}] := [a_{\alpha\beta}]^{-1} \quad (4)$$

we obtain the contra-variant components of the metric tensor. Explicitly, we have $a^{11} = a_{22}/\det a_{\alpha\beta}$, $a^{12} = -a_{12}/\det a_{\alpha\beta}$ and $a^{22} = a_{11}/\det a_{\alpha\beta}$. With these a dual basis can be constructed: From the co-variant base vectors \mathbf{a}_α the contra-variant counterparts

$$\mathbf{a}^\alpha := a^{\alpha\beta} \mathbf{a}_\beta \quad (5)$$

can be determined. We note that summation is implied on repeated indices. Note that $\mathbf{a}^\alpha \cdot \mathbf{a}^\beta = a^{\alpha\beta}$ and $\mathbf{a}_\alpha \cdot \mathbf{a}^\beta = \delta_\alpha^\beta$, where δ_α^β is the Kronecker symbol. The unit normal of \mathcal{S} at \mathbf{x} is given by

$$\mathbf{n} = \frac{\mathbf{a}_1 \times \mathbf{a}_2}{\|\mathbf{a}_1 \times \mathbf{a}_2\|}. \quad (6)$$

It can be shown that

$$\|\mathbf{a}_1 \times \mathbf{a}_2\| = \sqrt{\det a_{\alpha\beta}}. \quad (7)$$

The bases $\{\mathbf{a}_1, \mathbf{a}_2, \mathbf{n}\}$ and $\{\mathbf{a}^1, \mathbf{a}^2, \mathbf{n}\}$ can then be used to decompose any vector \mathbf{v} on \mathcal{S} , i.e.

$$\mathbf{v} = v^\alpha \mathbf{a}_\alpha + v_n \mathbf{n} = v_\alpha \mathbf{a}^\alpha + v_n \mathbf{n}, \quad (8)$$

where v_α denote the co-variant, and v^α the contra-variant components of \mathbf{v} . The derivative of the tangent vectors is given by

$$\mathbf{a}_{\alpha,\beta} = \frac{\partial \mathbf{a}_\alpha}{\partial \xi^\beta}. \quad (9)$$

Further, we require the so-called co-variant derivative of \mathbf{a}_α , which is defined by

$$\mathbf{a}_{\alpha;\beta} := \mathbf{a}_{\alpha,\beta} - \Gamma_{\alpha\beta}^\gamma \mathbf{a}_\gamma \quad (10)$$

where $\Gamma_{\alpha\beta}^\gamma$ are the Christoffel symbols of the second kind given by $\Gamma_{\alpha\beta}^\gamma = \mathbf{a}_{\alpha,\beta} \cdot \mathbf{a}^\gamma$. Introducing the identity tensor on \mathcal{S}

$$\mathbf{1} = \mathbf{a}_\alpha \otimes \mathbf{a}^\alpha = \mathbf{a}^\alpha \otimes \mathbf{a}_\alpha = \tilde{\mathbf{1}} - \mathbf{n} \otimes \mathbf{n}, \quad (11)$$

where $\tilde{\mathbf{1}}$ is the usual identity tensor⁵ in \mathbb{R}^3 , we can write

$$\mathbf{a}_{\alpha;\beta} = (\mathbf{n} \otimes \mathbf{n}) \mathbf{a}_{\alpha,\beta}. \quad (12)$$

Contracting with \mathbf{n} then yields

$$\mathbf{n} \cdot \mathbf{a}_{\alpha;\beta} = \mathbf{n} \cdot \mathbf{a}_{\alpha,\beta} =: b_{\alpha\beta} \quad (13)$$

which are the co-variant components of the curvature tensor $\mathbf{b} = b_{\alpha\beta} \mathbf{a}^\alpha \otimes \mathbf{a}^\beta$. The eigenvalues of this tensor are the principal curvatures of surface \mathcal{S} .

2.2 Membrane kinematics

Next, we consider the deformation of the membrane surface. We therefore distinguish between the deformed, current configuration \mathcal{S} and the undeformed, initial configuration \mathcal{S}_0 , see Fig. 1. Both surfaces are described by the relations of Sec. 2.1. For surface \mathcal{S} we use the lower case symbols \mathbf{x} , \mathbf{a}_α , $a_{\alpha\beta}$, \mathbf{a}^α , \mathbf{n} and $b_{\alpha\beta}$. For surface \mathcal{S}_0 we use the corresponding upper case symbols \mathbf{X} , \mathbf{A}_α , $A_{\alpha\beta}$, \mathbf{A}^α and \mathbf{N} .⁶ In order to characterize the deformation between surfaces \mathcal{S}_0 and \mathcal{S} consider the line element

$$d\mathbf{x} = \frac{\partial \mathbf{x}}{\partial \xi^\alpha} d\xi^\alpha = \mathbf{a}_\alpha d\xi^\alpha \quad (14)$$

and likewise $d\mathbf{X} = \mathbf{A}_\alpha d\xi^\alpha$. Contracting with \mathbf{A}^β yields $d\xi^\alpha = \mathbf{A}^\alpha \cdot d\mathbf{X}$, so that

$$d\mathbf{x} = (\mathbf{a}_\alpha \otimes \mathbf{A}^\alpha) d\mathbf{X}. \quad (15)$$

⁵A tilde is used here to indicate standard tensors in \mathbb{R}^3

⁶Here, the curvature tensor components $b_{\alpha\beta}$ are only needed on \mathcal{S} .

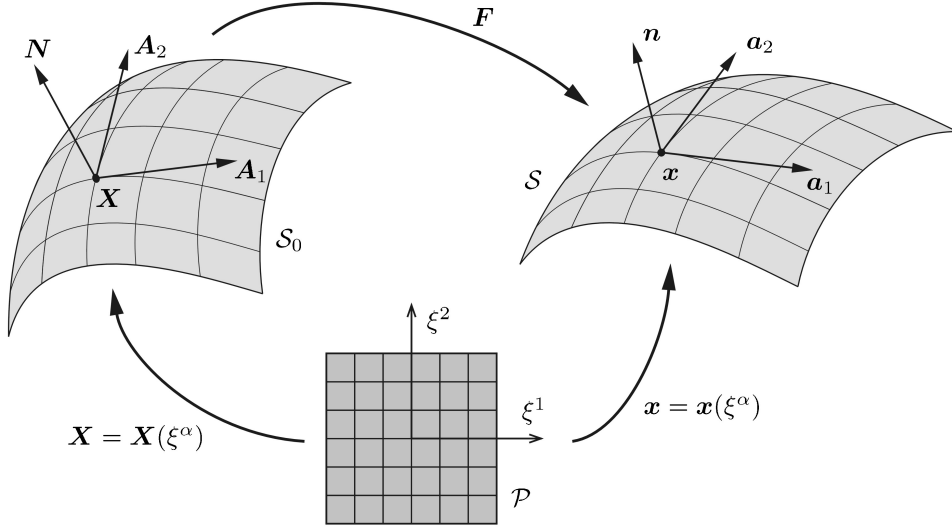


Figure 1: Mapping between parameter domain \mathcal{P} , reference surface \mathcal{S}_0 and current surface \mathcal{S}

Here the tensor

$$\mathbf{F} = \mathbf{a}_\alpha \otimes \mathbf{A}^\alpha \quad (16)$$

is the surface deformation gradient of the mapping $\mathbf{X} \rightarrow \mathbf{x}$. Likewise we find $\mathbf{F}^{-1} = \mathbf{A}_\alpha \otimes \mathbf{a}^\alpha$. Through \mathbf{F} we thus have the following transformations

$$\begin{aligned} \mathbf{a}_\alpha &= \mathbf{F} \mathbf{A}_\alpha, & \mathbf{A}_\alpha &= \mathbf{F}^{-1} \mathbf{a}_\alpha, \\ \mathbf{a}^\alpha &= \mathbf{F}^{-T} \mathbf{A}^\alpha, & \mathbf{A}^\alpha &= \mathbf{F}^T \mathbf{a}^\alpha. \end{aligned} \quad (17)$$

Given \mathbf{F} , we can introduce the right and left Cauchy-Green surface tensors and their inverses, i.e.

$$\begin{aligned} \mathbf{C} &= \mathbf{F}^T \mathbf{F} = a_{\alpha\beta} \mathbf{A}^\alpha \otimes \mathbf{A}^\beta, & \mathbf{C}^{-1} &= a^{\alpha\beta} \mathbf{A}_\alpha \otimes \mathbf{A}_\beta, \\ \mathbf{B} &= \mathbf{F} \mathbf{F}^T = A^{\alpha\beta} \mathbf{a}_\alpha \otimes \mathbf{a}_\beta, & \mathbf{B}^{-1} &= A_{\alpha\beta} \mathbf{a}^\alpha \otimes \mathbf{a}^\beta. \end{aligned} \quad (18)$$

Next, we discuss the surface stretch between surfaces \mathcal{S}_0 and \mathcal{S} . The area element $da \subset \mathcal{S}$ is defined by

$$da := \|(\mathbf{a}_1 d\xi^1) \times (\mathbf{a}_2 d\xi^2)\| = \|\mathbf{a}_1 \times \mathbf{a}_2\| d\Box, \quad (19)$$

where $d\Box := d\xi^1 d\xi^2$. A corresponding statement follows for $dA \subset \mathcal{S}_0$. In view of Eq. (7) we thus have the relations

$$\begin{aligned} dA &= J_A d\Box, & J_A &:= \sqrt{\det A_{\alpha\beta}}, \\ da &= J_a d\Box, & J_a &:= \sqrt{\det a_{\alpha\beta}}, \\ da &= J dA, & J &:= J_a/J_A. \end{aligned} \quad (20)$$

2.3 Momentum balance for membranes

From the balance of linear momentum the strong form equilibrium equation

$$\mathbf{t}_{;\alpha}^\alpha + \mathbf{f} = \mathbf{0}, \quad (21)$$

at $\mathbf{x} \in \mathcal{S}$ can be obtained (Steigmann, 1999). Here \mathbf{f} is a distributed surface force, that can be decomposed as

$$\mathbf{f} = f_\alpha \mathbf{a}^\alpha + p \mathbf{n} = f^\alpha \mathbf{a}_\alpha + p \mathbf{n} \quad (22)$$

where f_α and f^α are the co-variant and contra-variant in-plane components of \mathbf{f} and p is the out-of-plane pressure acting on \mathcal{S} . Further, \mathbf{t}^α denotes the internal traction acting on the internal surface $\perp \mathbf{a}^\alpha$. According to Cauchy's formula

$$\mathbf{t}^\alpha = \boldsymbol{\sigma} \mathbf{a}^\alpha, \quad (23)$$

where $\boldsymbol{\sigma}$ denotes the Cauchy stress tensor at $\mathbf{x} \in \mathcal{S}$, which we consider to be symmetric. We emphasize that \mathbf{t}^α is not a physical traction since \mathbf{a}^α is usually not normalized. In general, the stress tensor takes the form

$$\boldsymbol{\sigma} = \sigma^{\alpha\beta} \mathbf{a}_\alpha \otimes \mathbf{a}_\beta + \sigma^{3\alpha} (\mathbf{n} \otimes \mathbf{a}_\alpha + \mathbf{a}_\alpha \otimes \mathbf{n}) + \sigma^{33} \mathbf{n} \otimes \mathbf{n}. \quad (24)$$

For membranes it is typically assumed that $\sigma^{3\alpha} = \sigma^{33} = 0$, so that

$$\boldsymbol{\sigma} = \sigma^{\alpha\beta} \mathbf{a}_\alpha \otimes \mathbf{a}_\beta. \quad (25)$$

We denote this *the in-plane Cauchy stress tensor*. For convenience we consider the unit of $\boldsymbol{\sigma}$ as force per length, so that we can eliminate the membrane thickness from the formulation (see Sec. 2.4). We now find that $\mathbf{t}^\alpha = \sigma^{\beta\alpha} \mathbf{a}_\beta$ such that the co-variant derivative of \mathbf{t}^α becomes

$$\mathbf{t}_{;\alpha}^\alpha = \sigma^{\beta\alpha}_{;\alpha} \mathbf{a}_\beta + \sigma^{\beta\alpha} b_{\alpha\beta} \mathbf{n} \quad (26)$$

according to Eq. (13). Equilibrium equation (21) thus decomposes into

$$\begin{aligned} \sigma^{\beta\alpha}_{;\alpha} + f^\beta &= 0, & (\text{in-plane equilibrium}), \\ \sigma^{\alpha\beta} b_{\alpha\beta} + p &= 0, & (\text{out-of-plane equilibrium}). \end{aligned} \quad (27)$$

To close the problem, the usual Dirichlet and Neumann boundary conditions

$$\begin{aligned} \mathbf{u} &= \bar{\mathbf{u}} & \text{on } \partial_u \mathcal{S} \\ \mathbf{t} &= \bar{\mathbf{t}} & \text{on } \partial_t \mathcal{S} \end{aligned} \quad (28)$$

are considered on the membrane boundary $\partial \mathcal{S} = \partial_u \mathcal{S} \cup \partial_t \mathcal{S}$. Here, we suppose that the prescribed traction $\bar{\mathbf{t}} = \bar{t}^\alpha \mathbf{a}_\alpha$ is tangent to \mathcal{S} , since out-of-plane boundary forces, as well as out-of-plane line and point loads within the surface, lead to singularities in the membrane deformation and are therefore not considered in the present formulation. The traction on boundary $\partial_t \mathcal{S}$, according to Cauchy's formula, is given by

$$\mathbf{t} = \boldsymbol{\sigma} \mathbf{m}, \quad (29)$$

where $\mathbf{m} = m_\alpha \mathbf{a}^\alpha$ is the outward unit normal of $\partial_t \mathcal{S}$. It follows that $\mathbf{t} = m_\alpha \mathbf{t}^\alpha$.

2.4 Membrane constitution

The known 3D constitutive models can be adapted to the membrane. We therefore suppose a general elastic material relation of the form $\tilde{\boldsymbol{\sigma}} = \tilde{\boldsymbol{\sigma}}(\tilde{\mathbf{B}})$. For membranes it is useful to consider the decomposition $\tilde{\mathbf{B}} = \mathbf{B} + \lambda_3^2 (\mathbf{n} \otimes \mathbf{n})$, where λ_3 is the out-of-plane stretch, and $\tilde{\boldsymbol{\sigma}} = \boldsymbol{\sigma}/t + \sigma_{33} (\mathbf{n} \otimes \mathbf{n})$, where $\boldsymbol{\sigma}$ is the in-plane stress tensor defined in Eq. (25) and $t = \lambda_3 T$ denotes the current membrane thickness, for a given reference thickness T . Out of these considerations,

a relation between the membrane quantities \mathbf{B} and $\boldsymbol{\sigma}$ can be obtained. As an example we consider an incompressible Neo-Hooke material, given by

$$\tilde{\boldsymbol{\sigma}} = \tilde{\mu}\tilde{\mathbf{B}} + q\tilde{\mathbf{1}} , \quad (30)$$

where $\tilde{\mu}$ is the shear modulus and q denotes the Lagrange multiplier associated with the incompressibility constraint. For membranes, the model decomposes into

$$\begin{aligned} \boldsymbol{\sigma} &= (\tilde{\mu}\mathbf{B} + q\mathbf{1})T\lambda_3 , \\ \sigma_{33} &= \tilde{\mu}\lambda_3^2 + q . \end{aligned} \quad (31)$$

For incompressibility $\det \tilde{\mathbf{B}} = (J\lambda_3)^2 = 1$. Under the plane stress assumption $\sigma_{33} = 0$, we then find $q = -\tilde{\mu}/J^2$ and consequently

$$\boldsymbol{\sigma} = \frac{\mu}{J} \left(\mathbf{B} - \frac{\mathbf{1}}{J^2} \right) , \quad (32)$$

with $\mu := \tilde{\mu}T$. Componentwise, in the \mathbf{a}_α basis, this becomes

$$\sigma^{\alpha\beta} = \frac{\mu}{J} \left(A^{\alpha\beta} - \frac{a^{\alpha\beta}}{J^2} \right) . \quad (33)$$

Contracting with $a_{\beta\gamma}$, the components σ_β^α and $\sigma_{\alpha\beta}$ can be obtained.⁷

Another example are liquid, e.g. water, membranes governed by constant isotropic surface tension γ . In that case a constant stress tensor of the form

$$\sigma_\beta^\alpha = \gamma \delta_\beta^\alpha \quad (34)$$

is obtained. It can be seen that the in-plane equilibrium equation (27.1) is only satisfied for $f^\alpha = 0$. This implies that static water membranes cannot equilibrate in-plane loads, and are therefore unstable in-plane; a property that needs to be addressed in a computational formulation (see Sec. 3). The out-of-plane equation (27.2) now yields

$$2H\gamma + p = 0 , \quad 2H := b_\alpha^\alpha , \quad (35)$$

which is the well known Young-Laplace equation. A prominent feature of liquid membranes is that they form distinct contact angles. This angle is a consequence of a line force acting along the contact line. An example is shown in Sec. 4.5.

2.5 Membrane weak form

Next, we derive the weak form corresponding to equilibrium equation (21). Consider a kinematically admissible variation of \mathcal{S} , denoted $\mathbf{w} \in \mathcal{W}$, where \mathcal{W} denotes a suitable space for \mathbf{w} . Contracting Eq. (21) with \mathbf{w} and integrating over \mathcal{S} yields

$$\int_{\mathcal{S}} \mathbf{w} \cdot (\mathbf{t}_{;\alpha}^\alpha + \mathbf{f}) \, da = 0 \quad \forall \mathbf{w} \in \mathcal{W} . \quad (36)$$

Considering $\mathbf{w} = w_\alpha \mathbf{a}^\alpha + w \mathbf{n}$, this expands into

$$\int_{\mathcal{S}} w_\alpha (\sigma^{\alpha\beta}_{;\beta} + f^\alpha) \, da + \int_{\mathcal{S}} w (\sigma^{\alpha\beta} b_{\alpha\beta} + p) \, da = 0 \quad \forall \mathbf{w} \in \mathcal{W} , \quad (37)$$

⁷Due to the symmetry of $\sigma^{\alpha\beta}$ the ordering of indices does not matter in σ_β^α , i.e. $\sigma_\beta^\alpha = \sigma_\beta^\alpha$.

i.e. it splits into the in-plane and out-of-plane parts identified in Eq. (27). Such a split is useful if different approximation techniques are chosen for the in-plane and out-of-plane response. Using the divergence theorem for curved surfaces (Gurtin and Murdoch, 1975), the first in-plane term is rewritten into

$$\begin{aligned} \int_S w_\alpha \sigma^{\alpha\beta}_{;\beta} da &= \int_S (w_\alpha \sigma^{\alpha\beta})_{;\beta} da - \int_S w_{\alpha;\beta} \sigma^{\alpha\beta} da \\ &= \int_{\partial S} w_\alpha \sigma^{\alpha\beta} m_\beta ds - \int_S w_{\alpha;\beta} \sigma^{\alpha\beta} da , \end{aligned} \quad (38)$$

where $m_\alpha = \mathbf{m} \cdot \mathbf{a}_\alpha$ are the co-variant components of the unit normal \mathbf{m} on the line ∂S . Since $w^\alpha = 0$ on $\partial_u S$ and since $w_\alpha \sigma^{\alpha\beta} m_\beta = w_\alpha \bar{t}^\alpha$ on $\partial_t S$ expression (37) thus becomes

$$G_{\text{int}} - G_{\text{ext}} = 0 \quad \forall \mathbf{w} \in \mathcal{W} , \quad (39)$$

where

$$\begin{aligned} G_{\text{int}} &:= \int_S w_{\alpha;\beta} \sigma^{\alpha\beta} da - \int_S w \sigma^{\alpha\beta} b_{\alpha\beta} da , \\ G_{\text{ext}} &:= \int_S w_\alpha f^\alpha da + \int_{\partial_t S} w_\alpha \bar{t}^\alpha ds + \int_S w p da , \end{aligned} \quad (40)$$

are the internal and external virtual work contribution due to variation \mathbf{w} . Considering $w_\alpha = 0$ and $w = 0$ subsequently, the weak form can be decomposed into the weak forms

$$\begin{aligned} \int_S w_{\alpha;\beta} \sigma^{\alpha\beta} da - \int_S w_\alpha f^\alpha da - \int_{\partial_t S} w_\alpha \bar{t}^\alpha ds &= 0 \quad \forall w_\alpha \in \mathcal{W}_\alpha \quad (\text{in-plane}), \\ \int_S w \sigma^{\alpha\beta} b_{\alpha\beta} da + \int_S w p da &= 0 \quad \forall w \in \mathcal{W}_n \quad (\text{out-of plane}). \end{aligned} \quad (41)$$

Such a split is advantageous for the description of liquid membranes. Since liquid membranes are inherently unstable in-plane, they can be stabilized by providing additional stiffness via Eq. (41.1) without affecting the out-of-plane response. This is demonstrated in the examples of Sec. 4.4 and 4.5.

Otherwise, considering

$$w_{\alpha;\beta} = (\mathbf{w} \cdot \mathbf{a}_\alpha)_{;\beta} = \mathbf{w}_{;\beta} \cdot \mathbf{a}_\alpha + w b_{\alpha\beta} , \quad (42)$$

the two terms of G_{int} can be combined into

$$G_{\text{int}} = \int_S \mathbf{w}_{;\alpha} \cdot \sigma^{\alpha\beta} \mathbf{a}_\beta da . \quad (43)$$

It is noted that for this expression only single derivatives of variation \mathbf{w} and configuration \mathbf{x} are required, while in the decomposed formulation of Eq. (41) second derivatives of \mathbf{x} appear. Introducing the surface Kirchhoff stress tensor $\boldsymbol{\tau} = J\boldsymbol{\sigma}$, which eliminates one J from expression (33), the last equation can be rewritten into

$$G_{\text{int}} = \int_{S_0} \mathbf{w}_{;\alpha} \cdot \boldsymbol{\tau}^{\alpha\beta} \mathbf{a}_\beta dA . \quad (44)$$

Within framework (39), both dead and live loading can be considered. This is discussed further in Sec. 3.2. Beforehand, we discuss several useful membrane constraints.

2.6 Volume constraints

The volume of the domain \mathcal{D} enclosed by the membrane may be constrained. An example is a cell containing incompressible fluid. Formally, the volume constraint is written as

$$g_v := V_0 - V = 0 , \quad (45)$$

where V_0 and V denote the initial and current volumes enclosed by the initial and current membrane configurations. Since $dv = \mathbf{x} \cdot \mathbf{n} da/3$ and $dV = \mathbf{X} \cdot \mathbf{N} dA/3$, these can be computed by the surface integration

$$V = \frac{1}{3} \int_{\mathcal{S}} \mathbf{x} \cdot \mathbf{n} da , \quad V_0 = \frac{1}{3} \int_{\mathcal{S}_0} \mathbf{X} \cdot \mathbf{N} dA \quad (46)$$

These expressions are valid for closed surfaces, and care has to be taken when modeling open membranes. In this case one must account for the volume contribution associated with the missing surface. Eq. (45) can be included in the formulation by the Lagrange multiplier method. The Lagrange multiplier associated with the volume constraint is the internal membrane pressure p .

Remark 1: Eq. (45) is a global constraint on the entire system. This approach can be taken, if the medium enclosed by the membrane can be characterized by pressure and volume alone, as is the case for quasi-static conditions. If the fluid dynamics of the inside medium is relevant, the volume constraint needs to be considered as part of the fluid equations.

Remark 2: We note that the governing equations (39) and (45) can be derived from a variational principle for conservative systems. This is the case for the constitutive models discussed in Sec. 2.4 and for pressure loading of closed membranes surfaces.

2.7 Area constraints

Another useful constraint is a constraint on the membrane surface area. For example, red blood cells are known to conserve the surface area during deformation (Kloeppe and Wall, 2011). The area constraint can be formulated globally and locally. The global area constraint can be expressed as

$$g_a := A_0 - A = 0 , \quad (47)$$

with

$$A = \int_{\mathcal{S}} da , \quad A_0 = \int_{\mathcal{S}_0} dA . \quad (48)$$

The local area constraint needs to be expressed pointwise, by setting

$$g_a := 1 - J = 0 , \quad (49)$$

where J is defined by Eq. (20). The satisfaction of (49) implies the satisfaction of (47), but not vice versa. The local area constraint can be treated similarly as incompressible elasticity in 2D. The global area constraint can be treated in a similar manner than the volume constraint. An example is considered in Sec. 4.6.

2.8 Contact constraints

Contact is characterized by the impenetrability constraint

$$g_n \geq 0 , \quad (50)$$

where

$$g_n := (\mathbf{x} - \mathbf{x}_p) \cdot \mathbf{n}_p \quad (51)$$

denotes the normal gap between the membrane point $\mathbf{x} \in \mathcal{S}$ and the surface Γ of a neighboring obstacle. Here, the unit vector \mathbf{n}_p denotes the surface normal of Γ at the point \mathbf{x}_p , which is the solution of the minimum distance problem

$$\mathbf{x}_p(\mathbf{x}) = \left\{ \mathbf{y} \mid \min_{\forall \mathbf{y} \in \Gamma} \|\mathbf{x} - \mathbf{y}\| \text{ for } \mathbf{x} \in \mathcal{S} \right\} . \quad (52)$$

We note that this minimization can cause difficulties for complex surface geometries (Wriggers, 2006). Constraint (50) can be included in the membrane formulation by various methods. The simplest of these is the penalty formulation, which is considered in all the contact examples of Sec. 4. In this case the contact traction \mathbf{f}_c acting at $\mathbf{x} \in \mathcal{S}$ is given by

$$\mathbf{f}_c = \begin{cases} -\epsilon_n g_n \mathbf{n}_p , & g_n < 0 , \\ \mathbf{0} , & g_n \geq 0 , \end{cases} \quad (53)$$

where ϵ_n is the penalty parameter. The contact forces contribute to virtual work balance (39). This can be expressed by including

$$G_c = - \int_{\mathcal{S}} \mathbf{w} \cdot \mathbf{f}_c \, da \quad (54)$$

on the left hand side of Eq. (39). For two deformable membranes in contact, weak form (39) must be satisfied for each membrane, and contribution G_c is added correspondingly to each weak form. To avoid a surface bias it is advantageous to treat both contact pairs equivalently as is done in the *two-half-pass algorithm* of Sauer and De Lorenzis (2013).

3 Finite element discretization

The governing equations (39) and (45) are solved by the finite element (FE) method. The initial surface \mathcal{S}_0 is therefore discretized into a set of finite elements Ω_0^e that are defined by nodal points \mathbf{X}_I or control points in the case of isogeometric FE. The deforming membrane is then described by the motion of the nodal points $\mathbf{X}_I \rightarrow \mathbf{x}_I$, which corresponds to a Lagrangian FE description. The deformed configuration of element Ω_0^e is denoted Ω^e . Here we consider quadrilateral elements since these can be conveniently related to a master element in the parameter domain $\xi^\alpha \in [-1, 1]$.

3.1 Finite element interpolation

Within elements Ω_0^e and Ω^e , the geometry is approximated by the nodal interpolations

$$\mathbf{X} \approx \mathbf{X}^h = \sum_I N_I \mathbf{X}_I , \quad (55)$$

and

$$\mathbf{x} \approx \mathbf{x}^h = \sum_I N_I \mathbf{x}_I , \quad (56)$$

where $N_I = N_I(\xi^1, \xi^2)$ denotes the nodal shape function defined on the master element in parameter space. The summation is carried out over the n_{ne} nodes of the element. Here, the following quadrilateral elements are considered: 4-noded linear Lagrange elements, 9-noded

quadratic Lagrange elements, quadratic NURBS elements, and cubic T-spline elements. In principle, any other element type can also be considered. For isogeometric elements the shape functions are constructed via the Bézier extraction operation (Borden et al., 2011; Scott et al., 2011). According to Eq. (2), the tangent vectors are thus approximated by

$$\mathbf{a}_\alpha \approx \sum_I N_{I,\alpha} \mathbf{x}_I, \quad (57)$$

where $N_{I,\alpha} = \partial N_I / \partial \xi^\alpha$. Considering a Bubnov-Galerkin formulation the variation \mathbf{w} is approximated in the same way as the deformation, i.e.

$$\mathbf{w} \approx \sum_I N_I \mathbf{w}_I. \quad (58)$$

For shorthand notation, we rewrite Eqs. (55), (56) and (58) into

$$\mathbf{X} \approx \mathbf{N} \mathbf{X}_e, \quad \mathbf{x} \approx \mathbf{N} \mathbf{x}_e, \quad \mathbf{w} \approx \mathbf{N} \mathbf{w}_e, \quad (59)$$

where $\mathbf{N} := [N_1 \tilde{\mathbf{1}}, \dots, N_I \tilde{\mathbf{1}}, \dots]$ is a $(3 \times 3n_{\text{ne}})$ array with the usual identity tensor $\tilde{\mathbf{1}}$ and \mathbf{X}_e , \mathbf{x}_e , and \mathbf{w}_e are vectors containing the stacked nodal values for the element.⁸ In order to discretize the weak form we need to discretize w_α , w and $\mathbf{w}_{;\alpha}$. We find

$$\begin{aligned} w_\alpha &\approx \mathbf{w} \cdot \mathbf{a}_\alpha = \mathbf{w}_e^T \mathbf{N}^T \mathbf{a}_\alpha = \mathbf{w}_e^T \mathbf{N}^T \mathbf{N}_{,\alpha} \mathbf{x}_e \\ w &\approx \mathbf{w} \cdot \mathbf{n} = \mathbf{w}_e^T \mathbf{N}^T \mathbf{n} \\ \mathbf{w}_{;\alpha} &\approx \mathbf{N}_{,\alpha} \mathbf{w}_e \end{aligned} \quad (60)$$

where $\mathbf{N}_{,\alpha} := [N_{1,\alpha} \tilde{\mathbf{1}}, \dots, N_{I,\alpha} \tilde{\mathbf{1}}, \dots]$. Note that for a vector like \mathbf{w} , the co-variant derivative $\mathbf{w}_{;\alpha}$ coincides with the regular partial derivative $\mathbf{w}_{,\alpha}$. The surface normal \mathbf{n} is given through definition (6) and approximation (57). According to (13), the components of the curvature tensor become

$$b_{\alpha\beta} \approx \mathbf{n} \cdot \mathbf{N}_{,\alpha\beta} \mathbf{x}_e. \quad (61)$$

With the above expressions, we further find

$$w_{\alpha;\beta} \approx \mathbf{w}_e^T \left(\mathbf{N}_{,\beta}^T \mathbf{N}_{,\alpha} + \mathbf{N}^T (\mathbf{n} \otimes \mathbf{n}) \mathbf{N}_{,\alpha\beta} \right) \mathbf{x}_e \quad (62)$$

according to eq. (42).

3.2 Discretized weak form

The above expressions are now used to discretize the membrane weak form of Sec. 2.5. The surface integration is carried out over the element domains Ω^e and then summed over all n_{el} FE as

$$G_{\text{int}} = \sum_{e=1}^{n_{\text{el}}} G_{\text{int}}^e, \quad G_{\text{ext}} = \sum_{e=1}^{n_{\text{el}}} G_{\text{ext}}^e. \quad (63)$$

For the internal virtual work of eq. (44) we now have

$$G_{\text{int}}^e = \int_{\Omega_0^e} \mathbf{w}_{;\alpha} \cdot \tau^{\alpha\beta} \mathbf{a}_\beta \, dA \approx \mathbf{w}_e^T \int_{\Omega_0^e} \mathbf{N}_{,\alpha}^T \tau^{\alpha\beta} \mathbf{N}_{,\beta} \, dA \mathbf{x}_e \quad (64)$$

⁸Non-italic discrete arrays \mathbf{X} , \mathbf{x} , \mathbf{w} and \mathbf{N} should not be confused with italic field variables \mathbf{X} , \mathbf{x} , \mathbf{w} and \mathbf{N} .

according to approximations (57) and (60). Writing $G_{\text{int}}^e = \mathbf{w}_e^T \mathbf{f}_{\text{int}}^e$, we identify the internal FE force vector

$$\mathbf{f}_{\text{int}}^e = \int_{\Omega_0^e} \mathbf{N}_{,\alpha}^T \tau^{\alpha\beta} \mathbf{N}_{,\beta} dA \mathbf{x}_e . \quad (65)$$

As noted in Eq. (40.1), the internal virtual work can be split into in-plane and out-of plane contributions. At the element level these are

$$G_{\text{inti}}^e = \int_{\Omega_0^e} w_{\alpha;\beta} \tau^{\alpha\beta} dA , \quad G_{\text{into}}^e = - \int_{\Omega_0^e} w \tau^{\alpha\beta} b_{\alpha\beta} dA , \quad (66)$$

such that $G_{\text{int}}^e = G_{\text{inti}}^e + G_{\text{into}}^e$. In view of Eqs. (60), (61) and (62), the corresponding force vectors become

$$\begin{aligned} \mathbf{f}_{\text{inti}}^e &= \int_{\Omega_0^e} \tau^{\alpha\beta} \left(\mathbf{N}_{,\alpha}^T \mathbf{N}_{,\beta} + \mathbf{N}^T (\mathbf{n} \otimes \mathbf{n}) \mathbf{N}_{,\alpha\beta} \right) dA \mathbf{x}_e , \\ \mathbf{f}_{\text{into}}^e &= - \int_{\Omega_0^e} \tau^{\alpha\beta} \mathbf{N}^T (\mathbf{n} \otimes \mathbf{n}) \mathbf{N}_{,\alpha\beta} dA \mathbf{x}_e . \end{aligned} \quad (67)$$

For G_{ext} we consider external loading of the form $\mathbf{f} = \mathbf{f}_0/J + p \mathbf{n}$, where \mathbf{f}_0 and p are given loading parameters. The first corresponds to a dead force per reference area, the second to a live pressure. According to Eq. (40.2) we then have

$$G_{\text{ext}}^e = \int_{\Omega_0^e} \mathbf{w} \cdot \mathbf{f}_0 dA + \int_{\partial_t \Omega^e} \mathbf{w} \cdot \bar{\mathbf{t}} ds + \int_{\Omega^e} w p da , \quad (68)$$

which yields the external force vector

$$\mathbf{f}_{\text{ext}}^e = \int_{\Omega_0^e} \mathbf{N}^T \mathbf{f}_0 dA + \int_{\partial_t \Omega^e} \mathbf{N}^T \bar{\mathbf{t}} ds + \int_{\Omega^e} \mathbf{N}^T p \mathbf{n} da . \quad (69)$$

The original weak form (39) now yields the discretized version

$$\mathbf{w}^T [\mathbf{f}_{\text{int}} - \mathbf{f}_{\text{ext}}] = \mathbf{0} , \quad (70)$$

where \mathbf{f}_{int} and \mathbf{f}_{ext} are obtained from the assembly of the corresponding elemental force vectors, and \mathbf{w} is the kinematically admissible set of all nodal variations. These are zero for the nodes on the Dirichlet boundary $\partial_u \mathcal{S}$. For the remaining nodes, Eq. (70) implies

$$\mathbf{f} := \mathbf{f}_{\text{int}} - \mathbf{f}_{\text{ext}} = \mathbf{0} , \quad (71)$$

which is the discretized equilibrium equation that needs to be solved for the unknown nodal positions \mathbf{x} ; see Sec. 3.5.

We note, that in this formulation no mapping of derivatives between master and current configuration is required. Also no introduction of local, cartesian bases are needed. The formulation thus is straight forward and efficient to implement.

3.3 Contact contributions

The proposed membrane model can be easily extended to include contact, provided a 3D contact algorithm is available. The contact contribution (54) simply yields the force vector

$$\mathbf{f}_c^e = - \int_{\Omega_k^e} \mathbf{N}^T \mathbf{f}_c da , \quad (72)$$

that needs to be included in Eq. (71). For details on the the FE implementation of Eq. (72) we refer to Sauer and De Lorenzis (2013).

3.4 Discretized volume and area constraints

The volume, enclosed by the discretized membrane surface, is obtained as

$$V = \frac{1}{3} \sum_{e=1}^{n_{el}} \int_{\Omega^e} \mathbf{n}^T \mathbf{N} da_{\mathbf{x}_e} \quad (73)$$

according to Eq. (46). For the volume constraint, $g_v = V_0 - V = 0$, V_0 can be considered as an externally prescribed volume, e.g. during inflation, or as the initial value of V . For the global area constraint, we simply evaluate Eqs. (47) and (48) by elementwise integration.

3.5 Solution method

The volume constraint is included in the formulation by the Lagrange multiplier method. The Lagrange multiplier associated with the constraint is the pressure, p , acting on membrane. Combining (45) with (71) leads to the system

$$\begin{aligned} \mathbf{f}(\mathbf{x}, p) &= \mathbf{0} , \\ g_v(\mathbf{x}) &= 0 , \end{aligned} \quad (74)$$

that needs to be solved for the unknown nodal position \mathbf{x} and pressure p . Due to the nonlinearities of the model, this is solved with Newton's method. Therefore, the linearization of \mathbf{f} and g_v w.r.t. \mathbf{x} and p are needed. This is discussed in Appendices A and B. For the area constraint, a similar setup is obtained. In this case, the Lagrange multiplier corresponds to an in-plane pressure that affects the in-plane stress state.

3.6 Hydrostatic pressure

In some applications, the pressure p may vary locally. In static examples this is typically due to gravity. An example is the hydrostatic pressure distribution in a water-filled membrane. In this case, we have

$$p = p_v + p_h , \quad (75)$$

where p_h is the hydrostatic, height dependent, pressure and p_v is the pressure associated with the volume constraint. The former is simply written as

$$p_h = \rho \mathbf{g} \cdot \mathbf{x} \quad (76)$$

where ρ is the density of the pressure causing medium, and \mathbf{g} is the gravity vector.⁹ The value of p_v is then the (constant) datum pressure at the origin.

3.7 Numerical quadrature

In parameter space, each element is defined on the master domain $\xi^\alpha \in [-1, 1]$, $\alpha = 1, 2$. The integrals from above are mapped to the master domain using transformations (20). Integration is then carried out with standard Gaussian quadrature on the master domain.

⁹typically $\mathbf{g} = -[0, 0, g]^T$, where g is the gravity constant

3.8 Monitoring compression

Membranes do not support in-plane compression. The absence of physical bending stiffness leads to buckling of the structure, known as wrinkling in the case of membranes. To avoid membrane compression in our formulation during computations, we simply monitor the minimum principal stress

$$\sigma_{\min} = \frac{I_1}{2} - \sqrt{\frac{I_1^2}{4} - I_2}, \quad (77)$$

where $I_1 = \text{tr } \boldsymbol{\sigma} = \sigma_\alpha^\alpha$ and $I_2 = \det \boldsymbol{\sigma} = \det \sigma_\beta^\alpha$ are the two invariants of the surface stress tensor. We note that $\sigma_{\min} < 0$ does not imply the automatic failure of the discretize membrane structure as some numerical bending stiffness may be present. More involved wrinkling criteria can be found in the literature, see [Lu et al. \(2001\)](#) and [Youn and Lee \(2006\)](#).

4 Numerical examples

The proposed membrane model is illustrated by several examples, considering both solid and liquid membranes under dead, pressure, and volume loading. Standard linear and quadratic Lagrange finite elements as well as quadratic NURBS and cubic T-spline finite elements, providing C^1 - and C^2 -continuous surface descriptions, respectively, are used.

4.1 Inflation of a spherical balloon

We first consider the inflation of a spherical rubber balloon and use it for validation, since an analytical solution exists for this problem. The rubber behavior is described by the incompressible Neo-Hookean material model (30). The finite element model of the balloon, modeled as 1/8th of a sphere, is shown in Fig. 2a. Appropriate boundary conditions are provided to main-

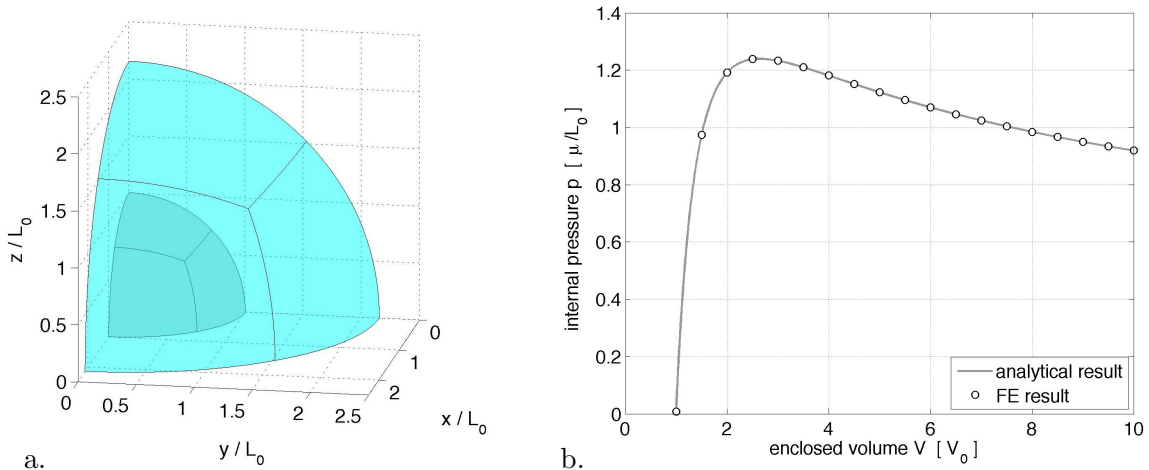


Figure 2: Inflated balloon: (a) initial and current configuration (for $V = 10 V_0$); (b) pressure-volume relation for $V \in [1 \ 10]V_0$ (FE result for 3 quadratic FE).

tain the symmetry of the inflating structure. The relation between current and initial radius is denoted $r = \lambda R$. The circumference of the balloon, proportional to r , is thus stretched by λ such that the surface deformation gradient is $\mathbf{F} = \lambda \mathbf{1}$ and the area change is given by $J = \lambda^2$.

Due to incompressibility this results in the thickness change $t = T/J$. According to Eq. (32), the in-plane normal stress within the balloon thus is $\tilde{\sigma} = \sigma/t = \tilde{\mu}T(1 - \lambda^{-6})/t$, which is equal to the well-known formula $\tilde{\sigma} = pr/2/t$. We thus obtain the pressure-stretch relation

$$\frac{pR}{\tilde{\mu}T} = 2\left(\frac{1}{\lambda} - \frac{1}{\lambda^7}\right), \quad (78)$$

or, equivalently, the pressure-volume relation

$$\frac{pR}{\tilde{\mu}T} = 2\left(\left(\frac{V_0}{V}\right)^{\frac{1}{3}} - \left(\frac{V_0}{V}\right)^{\frac{7}{3}}\right), \quad (79)$$

where $V_0 = 4\pi R^3/3$ is the initial balloon volume. The $p - V$ relation is shown in Fig. 2b. The pressure increases quickly, peaks and then decreases gradually. This behavior is typical for the inflation of rubber membranes. The FE computation of such problems should therefore be carried out by prescribed volume loading instead of prescribed pressure loading. The proposed FE formulation can capture the analytical behavior very nicely. This is shown by the convergence plot of Fig. 3a. Here, the number of Gaussian quadrature points per elements are

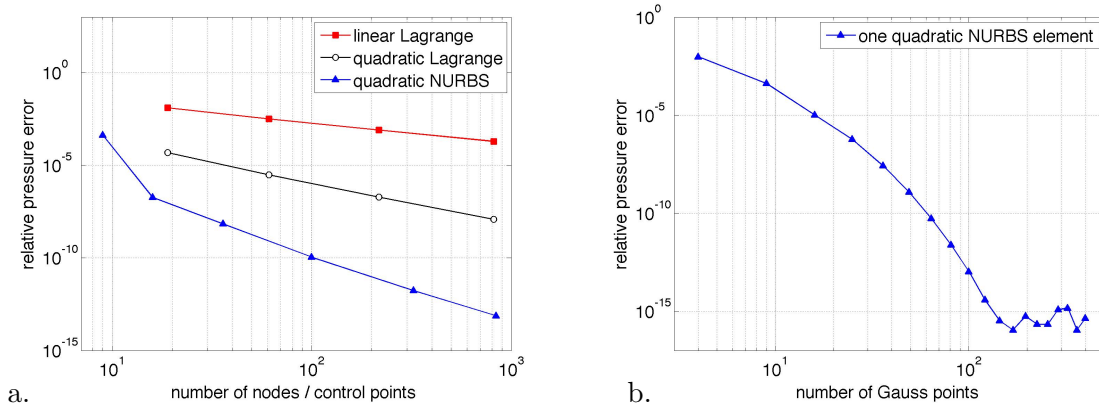


Figure 3: Inflated balloon: convergence of the pressure at $V = 10V_0$: (a) convergence with mesh size; (b) NURBS convergence with quadrature accuracy.

2×2 for linear Lagrange and 3×3 for quadratic Lagrange and NURBS elements. Since NURBS elements describe the spherical geometry exactly, they can solve the problem exactly with only one element – provided sufficiently many quadrature points are used. This is shown in Fig. 3b. The results shown here validate the proposed membrane formulation.

Fig 4 shows the deformed FE meshes and the error in the membrane stress σ for the three different element types considered here. As is seen, the error is smallest for NURBS FE. It reaches machine precision for 12×12 Gauss points.

4.2 Inflation of a square sheet

As a second example we consider a square membrane sheet with dimension $4L_0 \times 4L_0$, apply an isotropic pre-stretch of $\lambda_0 = 1.05$ to provide initial out-of-plane stiffness, and then inflate the structure by a prescribed volume, as is shown in Fig. 5.

Fig. 6a shows the pressure-volume relation for the three considered elements. The accuracy is

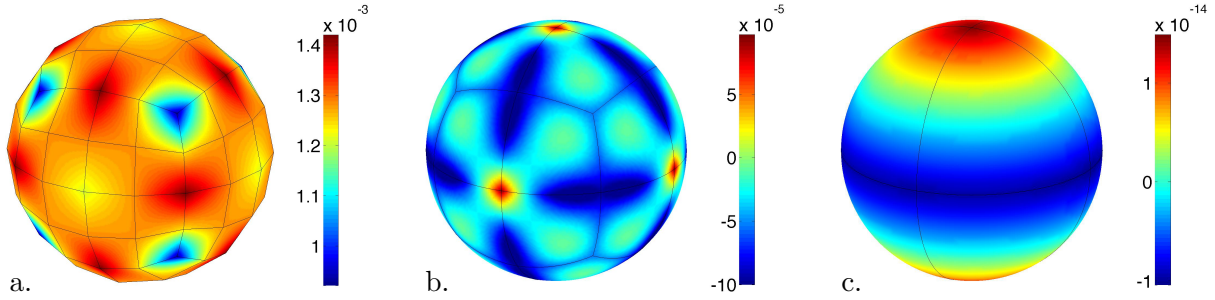


Figure 4: Inflated balloon: Error in the in-plane stress $\sigma = pr/2$ for: (a) 8×12 linear FE, (b) 8×3 quadratic FE, (c) 8×1 NURBS FE. The number of Gauss points is (a) 2×2 , (b) 3×3 , (c) 12×12

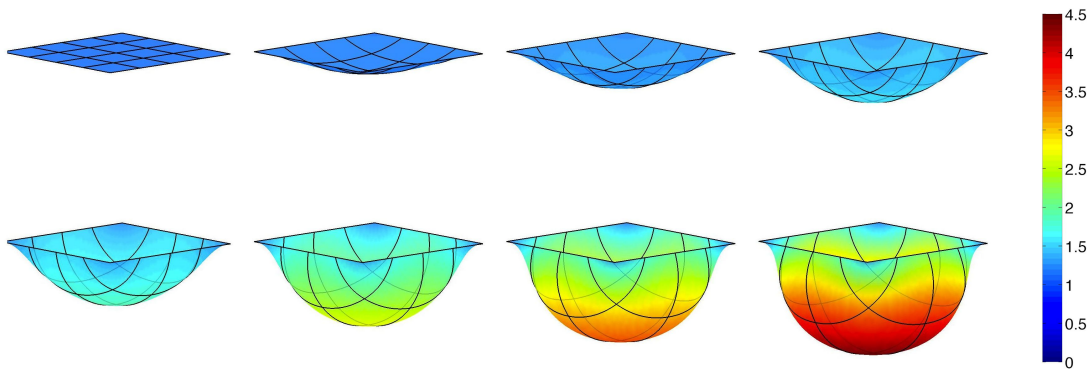


Figure 5: Inflated square sheet: configurations for $V = \{0, 1, 2, 3, 4, 6, 8, 10\}V_0$, where $V_0 = 4L_0^3$. The coloring shows the area stretch J (which is identical to the thickness decrease).

highest for NURBS elements and lowest for linear elements. This is seen by the convergence behavior of the different element types, shown in Fig. 6b.

Fig. 7 shows the deformed sheet for a prescribed volume of $V = 5000 V_0$ for the three element types. As seen, all element types can accommodate enormous deformations, even for relatively coarse meshes. The comparison with the fine NURBS mesh in Fig. 8a shows that there are still considerable inaccuracies present in all three formulations. The NURBS result is fully C^1 -continuous. In the example, particularly large deformation occur at the bottom and in the corners of the sheet, as is seen in the close-up of Fig. 8b. The deformation in the corner shown a tendency towards wrinkling. We observed that a further mesh refinement led to non-convergent Newton behavior, indicating instabilities. A computational scheme for wrinkling is required to handle this case.

4.3 Contact between balloon and cushion

The third example considers a spherical, water-filled balloon in contact with a cushion. The balloon is loaded by hydrostatic pressure loading. The cushion is modeled by a square sheet that is fixed along the boundary and supported by internal pressure arising from constraining the volume beneath the sheet. The initial size of the sheet is $2R \times 2R$, where R is the undeformed radius of the balloon. Both, balloon and sheet are modeled by material law (30) considering equal μ . They are both pre-stretched isotropically by $\lambda_0 = 1.1$, i.e. the constrained balloon

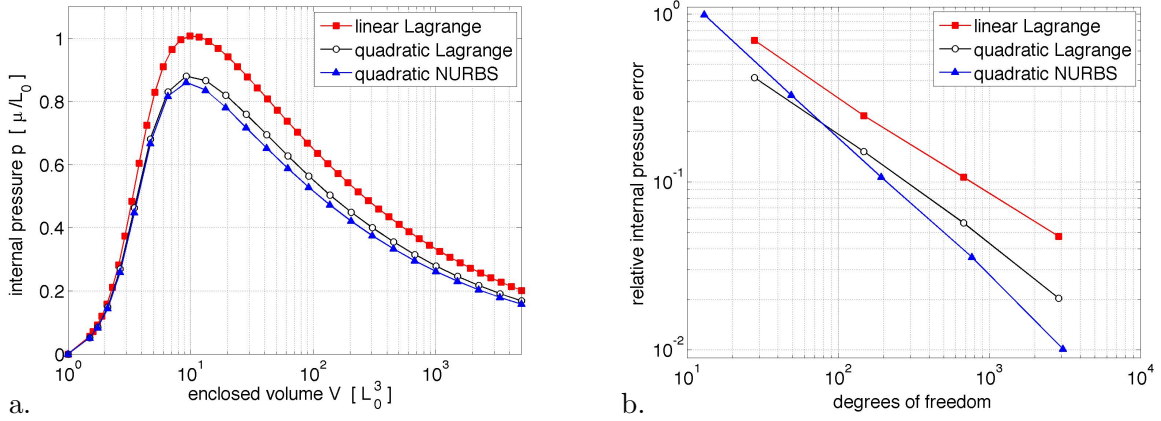


Figure 6: Inflated square sheet: (a) pressure-volume relation; (b) pressure convergence at $V = 5000V_0$ (compared to a quadratic NURBS mesh with 23233 dofs).

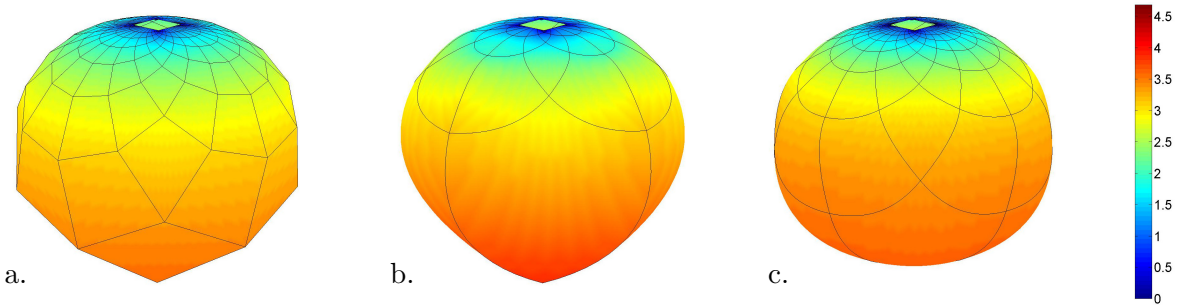


Figure 7: Inflated square sheet: deformation at $V = 5000V_0$ for (a) 8×8 linear elements, (b) 4×4 quadratic elements, and (c) 8×8 NURBS elements. The color shows the area stretch J displayed as $\log_{10} J$.

volume is $V_0 = 4\pi(\lambda_0 R)^3/3$. The problem is computed by gradually increasing the gravity level, g , pulling on the water inside the balloon. Quadratic finite elements are used. Contact is modeled by the two-half-pass contact algorithm (Sauer and De Lorenzis, 2013) considering the penalty method (see Sec. 2.8). In principle, any 3D contact algorithm can be applied straight forwardly to the proposed membrane formulation. Fig. 9 shows the deformation of balloon and cushion for various gravity levels. As shown, the deformation becomes very large, which makes the problem very challenging. The example is interesting as it involves large deformations, contact, pressure loading, hydrostatic loading and two volume constraints.

4.4 Growth of a hemispherical water droplet

As a validation of the formulation for liquid membranes, we consider the growth of a hemispherical droplet resting on a rigid substrate and maintaining a contact angle of 90° . The influence of gravity is neglected in order to provide an analytical comparison result. The problem is similar to the balloon inflation example (Sec. 4.1), and the same FE meshes are used. For a liquid water membrane the membrane stress is given by Eq. (34), i.e. the stress is deformation independent.

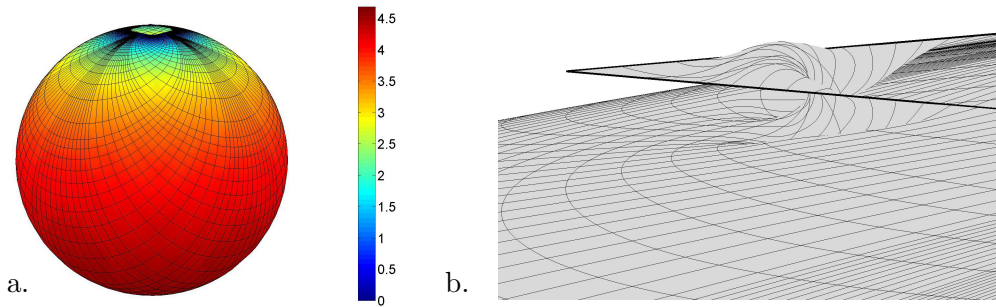


Figure 8: Inflated square sheet: deformation at $V = 5000 V_0$ for 88×88 NURBS elements: (a) overall deformation, (b) deformation at the corner.

This implies that only the out-of-plane but not the in-plane forces provide stiffness and the formulation is unstable in itself. The formulation can be stabilized by adding deformation dependent in-plane forces through Eq. (67.1). These forces should not influence the out-of-plane behavior such that the original liquid membrane formulation remains unaffected. We simply use the incompressible Neo-Hookean model to provide the additional in-plane stability. The Neo-Hookean material parameter μ then becomes a numerical stability parameter that should not affect the physical results. The internal forces acting on the finite element nodes are then simply given by

$$\mathbf{f}_{\text{int}}^e = \mathbf{f}_{\text{int}}^e(\sigma_{\text{liquid}}^{\alpha\beta}) + \mathbf{f}_{\text{inti}}^e(\sigma_{\text{solid}}^{\alpha\beta}) . \quad (80)$$

In the absence of gravity, the pressure-volume relation is obtained analytically, similarly to the balloon example of Sec. 4.1. Setting $\sigma = pr/2 = \gamma$, with $r = \lambda R$ and $V = \lambda^3 V_0$, we find

$$\frac{pR}{\gamma} = 2 \left(\frac{V_0}{V} \right)^{\frac{1}{3}} . \quad (81)$$

Since the pressure remains positive (and is thus stabilizing the structure) the volume can also be decreased. The computed pressure and the convergence of the proposed finite element formulation to the analytical result are shown in Fig. 10. Several values for the numerical stability parameter μ are considered. They all converge to the desired analytical result. Quadratic Lagrange and NURBS elements are considered, and it is seen that the NURBS formulation converges much faster. This is attributed to the higher surface continuity that appears in $\mathbf{f}_{\text{inti}}^e$ according to Eq. (67.1). Decreasing μ improves the accuracy. A more detailed analysis of the model proposed in Eq (80) along with the effect of parameter μ is considered in Sauer (2013b).

4.5 Liquid droplet on a rigid substrate

The next example examines a static water droplet in contact with a rigid substrate. Three cases are considered, which examine the influence of gravity, the contact angle and substrate roughness. Initially, prior to loading and contact, the droplet is spherical. We denote the initial radius R , and the initial volume $V_0 := 4\pi R^3/3$. The water inside the droplet is considered incompressible such that the volume remains constant during deformation. The weight of the water causes hydrostatic pressure loading of the membrane leading to contact with the substrate. The liquid membrane model is stabilized according to (80).

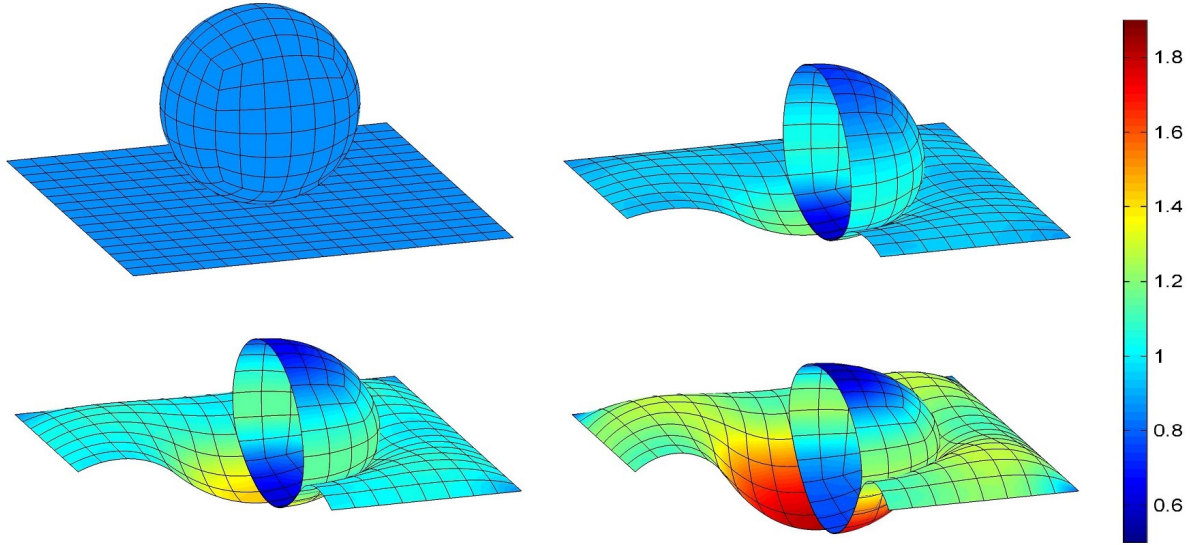


Figure 9: Cushion contact: configurations at $\rho g = \{0, 0.4, 0.8, 1.6\}\mu/R$. The coloring shows the stress invariant $I_1 = \text{tr } \boldsymbol{\sigma} = \sigma_\alpha^\alpha$ normalized by μ . Here $\epsilon_n = 2000 \mu/R$.

4.5.1 Influence of gravity

We first consider a contact angle of 180° . Fig. 11 shows the computed droplet deformation for various gravity values considering different FE formulations. T-Spline elements are used here to ensure a C^2 -continuous description across the entire surface (apart from two degenerate points at the top and bottom). As the gravity level increases the droplet spreads out on the substrate. Contact is modeled according to Sec. 2.8 using a penalty parameter $\epsilon_n \geq 5000\gamma/R$. Stability parameter μ is set to 0.005γ . The coloring in Fig. 11 shows the membrane stress component $I_1 = a_{\alpha\beta}(\sigma_{\text{liquid}}^{\alpha\beta} + \sigma_{\text{solid}}^{\alpha\beta})$, even though, according to (80), the stabilization term is only added to the in-plane but not to the out-of-plane response. (Plotting only $\hat{I}_1 = a_{\alpha\beta} \sigma_{\text{liquid}}^{\alpha\beta}$, yields $\hat{I}_1 = 2\gamma$ to machine precision in computations, which is physically correct but less interesting to look at.) Therefore, I_1 is not a physical error measure but rather a measure of the variational inconsistency introduced by the stabilization term. The figure shows that this consistency error is less than 2.5% in the case of quadratic Lagrange elements (Fig 11, top.) and less than 1% in the case of cubic T-splines (Fig 11, bottom). In both cases the errors increase along with ρg . In the case of Lagrange elements the largest errors are found at the element boundaries, where the formulation is only C^0 -continuous. For the T-spline case, which is C^2 -continuous, the error is uniformly spread over the surface. These errors are a consequence of the very coarse finite element meshes considered here. They will vanish under mesh refinement (cf. Fig. 10). This is studied in detail in Sauer (2013b).

4.5.2 Influence of the contact angle

A distinct feature of liquid membranes is that they can form sharp contact angles at the contact boundary. In this case, the membrane surface forms a kink at the contact boundary. These surface discontinuities are associated with out-of-plane line forces. Such forces can be easily included by applying a uniform line load \mathbf{q}_c along selected line finite elements, similar to the

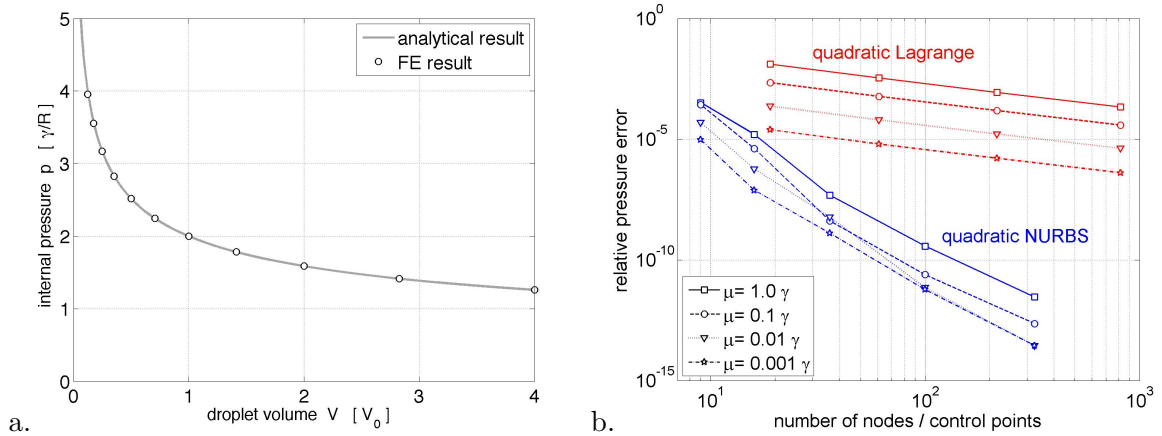


Figure 10: Growing liquid droplet: (a) pressure-volume relation for $V \in [1/8 \ 4]V_0$ (FE result for 12 quadratic FE with $\mu = 0.01\gamma$); (b) convergence behavior for $V = 4V_0$ and various μ , considering 3×3 Gaussian quadrature points.

application of $\bar{\mathbf{t}}$ in Eq. (69). This is shown in Fig. 12. Here, the surface tension of the free droplet surface and the surface tension at the contact interface are considered equal, and denoted γ . The contact angles $\theta_c = 120^\circ$ and $\theta_c = 60^\circ$ are thus obtained for a fixed line load \mathbf{q}_c with magnitude γ and $\sqrt{3}\gamma$, respectively, that is pulling outward along the bisecting angle, i.e. 60° and 30° . The figure shows that the consistency error in I_1 remains below 1% for the considered discretization.

Remark: Here, the line load \mathbf{q}_c has been applied to the line elements along the equator of the initially spherical droplet. A computational procedure for this, that accounts also for varying \mathbf{q}_c , is developed and assessed in Sauer (2013b). There, it is also shown that, for liquids, the initial location of the contact line can be chosen to coincide with the mesh without loss of generality. In Fig. 12, quadratic Lagrange elements are considered. In the case of NURBS elements, patch boundaries or knot insertion should be considered to create C^0 -continuous lines where kinks can form.

4.5.3 Influence of the surface roughness

The proposed membrane formulation is suitable to study the influence of surface roughness on liquid droplet contact. As an example, we consider the case from Fig. 12a (with $\theta_c = 180^\circ$, $V_0 = 4\pi R^3/3$ and $\rho g = 2\gamma/R^2$) and replace the flat surface by the rough surface shown in Fig. 13a that is taken from Sauer and Holl (2013). Here the distance between neighboring asperities is $0.2R$; their height is $0.1R$. The computational solution for this case is shown in Fig. 13b & c. It is observed that less than 7% of the bottom surface is in actual contact, while the remaining surface is suspended between the asperities. This wetting state, known as the Cassie-Baxter state, is a consequence of the strong hydrophobicity caused by the large contact angle. The small contact area leads to very high contact pressures above the asperities. To model this accurately a very large contact penalty parameter is needed. The consistency errors in I_1 are largest in the contact surface above the asperities. In those locations the discretization is still very coarse: Due to the small contact area, only few finite elements per asperity are in contact. If the contact angle is reduced, the local contact spot will spread down the asperities until eventually the entire rough substrate is wetted. This is partly shown for a single asperity in Sauer (2013b).

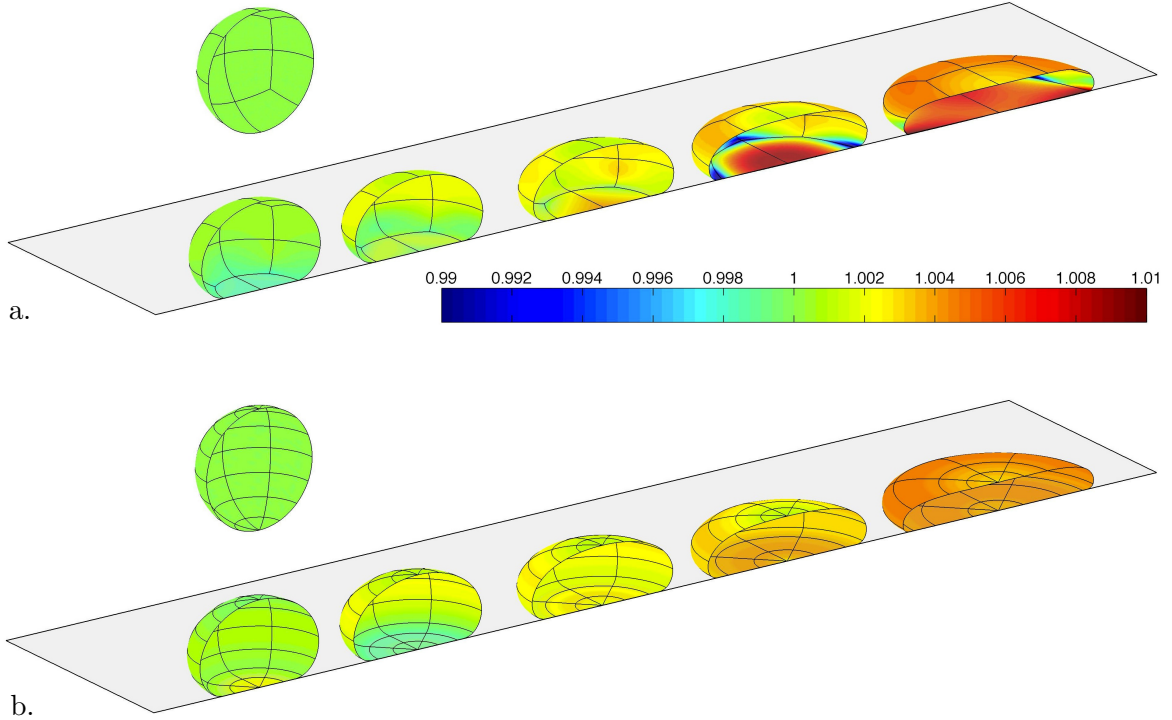


Figure 11: Liquid droplet contact: droplet deformation for $\rho g = \{1, 2, 4, 8, 20\}\gamma/R^2$, each with identical volume and $\mu = 0.005\gamma$: (a) quadratic Lagrange elements, (b) cubic T-spline elements. The color shows the membrane stress $I_1/2$ normalized by the surface tension γ . In theory $I_1/(2\gamma) = 1$.

We note, that the contact computation for liquid droplets is not a trivial task to perform. Low values for the stability parameter μ can lead to a loss of convergence. For the presented computations we have found the following procedure successful: We first increased ρg iteratively to its desired value, using a high μ and low ϵ_n . Then we decreased μ and increased ϵ_n iteratively until the accuracy is satisfactory. If convergence problems are encountered, a refinement of the FE mesh is considered.

4.6 Area constraint versus volume constraint

The last example considers the global area constraint of Sec. 2.7 and compares it with the global volume constraint of Sec. 2.6. Therefore a spherical rubber balloon, pressurized such that initially $\lambda_0 = 1.1$, is pinched between two rigid, flat surfaces. Fig. 14 shows the deformation for the two cases. In case of the area constraint, the volume of the balloon decreases during deformation. In case of the volume constraint, the surface area increases during deformation.

5 Conclusion

A novel computational formulation that is suitable for both solid and liquid, i.e. surface-tension-driven, membranes is presented. The theory, outlined in Sec. 2, is based on the differential geometry of curved surfaces, allowing for a very general formulation that accounts for large deformations and general material laws. Curvilinear coordinates are used to formulate the surface

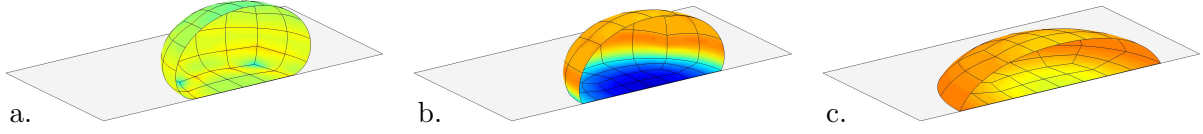


Figure 12: Liquid droplet contact: droplet deformation for the contact angles (a) $\theta_c = 180^\circ$, (b) $\theta_c = 120^\circ$ and (c) $\theta_c = 60^\circ$, all for $V_0 := 4\pi R^3/3$, $\rho g = 2\gamma/R^2$, $\mu = 0.005\gamma$ and $\epsilon_n = 5000\gamma/R$. The colors show $I_1/(2\gamma)$ in the same range as in Fig. 11.

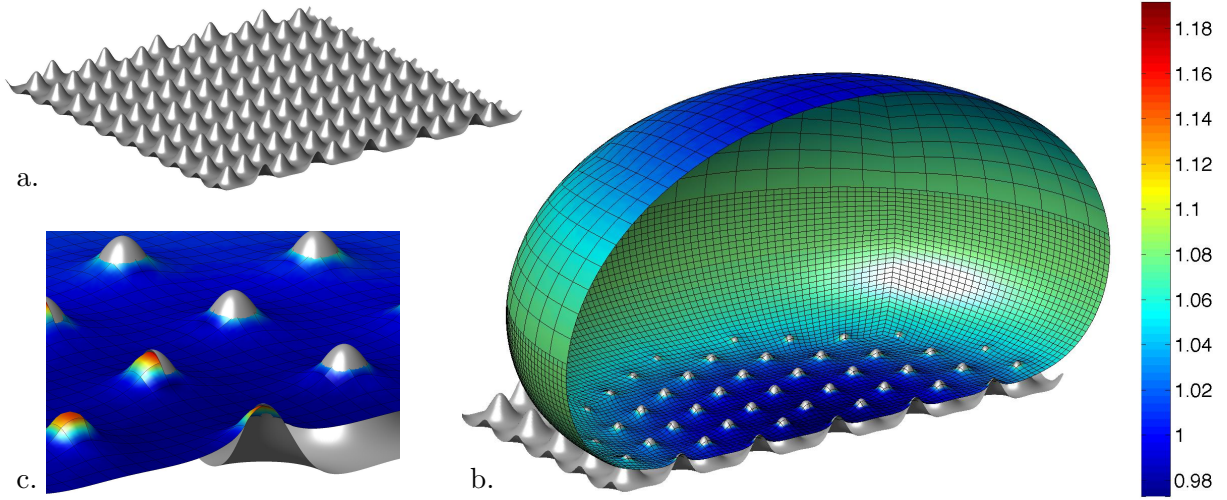


Figure 13: Liquid droplet contact: droplet deformation due to surface roughness: (a) surface model, (b) droplet deformation and error measure $I_1/(2\gamma)$, (c) enlargement of b that also partly shows the substrate surface (and its penetration into the droplet caused by the penalty regularization). Here, $\theta_c = 180^\circ$, $V_0 = 4\pi R^3/3$, $\rho g = 2\gamma/R^2$, $\mu = 0.2\gamma$ and $\epsilon_n = 1.07 \cdot 10^5\gamma/R$.

geometry, kinematics, constitution, and balance laws. The governing strong and weak forms are split into the in-plane and out-of-plane parts, allowing the use of different approximation techniques for both parts and an elegant treatment of liquid membranes. Also, the consideration of deformation-dependent pressure loading comes naturally within the proposed formulation. Various constraints imposed upon the membranes can be handled by the theory, including volume, area, and contact constraints.

The membrane formulation is discretized using nonlinear finite elements. This results in a very efficient formulation that only uses three degrees of freedom per surface node and avoids the use of local cartesian coordinate systems and the transformation of derivatives. This is discussed in Sec. 3.

The capabilities of the formulation are demonstrated by several challenging examples in Sec. 4. Linear Lagrange, quadratic Lagrange, quadratic NURBS, and cubic T-spline finite elements are considered for the discretization. Constraints are imposed using the Lagrange multiplier method in the case of volume and area constraints and the penalty method for contact constraints. The inflation of a balloon and the growth of a droplet are used to validate the solid and liquid membrane formulations and they both yield excellent results. Comparing the different finite element types, the examples show that large accuracy gains lie between linear and quadratic

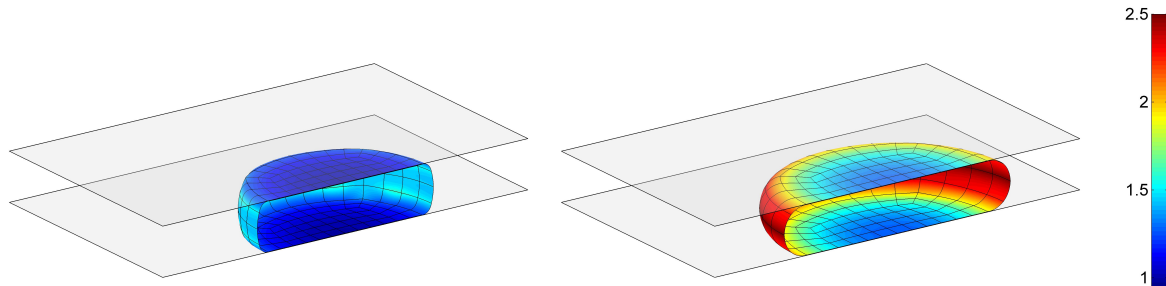


Figure 14: Pinched rubber balloon: global area constraint (left) vs. global volume constraint (right). The color shows the surface stretch J . For the area constraint this correctly averages to $J = \lambda_0^2 = 1.21$. Here $\epsilon_n = 1000 \mu/R$.

Lagrange, and between quadratic Lagrange and isogeometric finite elements.

The presented membrane formulation has been successfully applied to liquid droplets in this paper, including contact angles and rough surface contact, but a rigorous analysis is still needed to assess the approach proposed in Eq. (80), see Sauer (2013b). Another important extension to the present formulation is the inclusion of bending stiffness, which can be present in both fluid and solid films. In the latter case this should lead naturally to a rotation-free shell formulation, which can be suitably handled by isogeometric finite elements. A further interesting extension is the consideration and development of different membrane material laws. Such a development is especially important for the case of biological membranes, which are often characterized by complex material behavior.

A Consistent linearization of various quantities

For Newton's method we need to linearize the kinematical quantities of the discrete system at \mathbf{x} in the direction $\Delta \mathbf{x}$. This is done at the FE level.

A.1 Linearization of \mathbf{a}_α

According to Eq. (57) we have

$$\Delta \mathbf{a}_\alpha = \mathbf{N}_{,\alpha} \Delta \mathbf{x}_e . \quad (82)$$

A.2 Linearization of $a_{\alpha\beta}$

With definition (3) follows

$$\Delta a_{\alpha\beta} = (\mathbf{a}_\alpha \cdot \mathbf{N}_{,\beta} + \mathbf{a}_\beta \cdot \mathbf{N}_{,\alpha}) \Delta \mathbf{x}_e . \quad (83)$$

A.3 Linearization of J

The change ΔJ can be written as

$$\Delta J = \frac{\partial J}{\partial \mathbf{a}_\alpha} \cdot \Delta \mathbf{a}_\alpha , \quad (84)$$

where

$$\frac{\partial J}{\partial \mathbf{a}_\alpha} = J \mathbf{a}^\alpha . \quad (85)$$

Thus

$$\Delta J = J \mathbf{a}^\alpha \cdot \mathbf{N}_{,\alpha} \Delta \mathbf{x}_e . \quad (86)$$

A.4 Linearization of $a^{\alpha\beta}$

From Eq. (5) and the formula

$$a^{\alpha\beta} = \frac{1}{a} e^{\alpha\gamma} a_{\gamma\delta} e^{\delta\beta} , \quad a := \det a_{\alpha\beta} , \quad (87)$$

where

$$[e^{\alpha\beta}] = \begin{bmatrix} 0 & 1 \\ -1 & 0 \end{bmatrix} \quad (88)$$

is the unit alternator, we find

$$\Delta a^{\alpha\beta} = m^{\alpha\beta\gamma\delta} \mathbf{a}_\gamma \cdot \mathbf{N}_{,\delta} \Delta \mathbf{x}_e , \quad (89)$$

with

$$m^{\alpha\beta\gamma\delta} = \frac{1}{a} (e^{\alpha\gamma} e^{\beta\delta} + e^{\alpha\delta} e^{\beta\gamma}) - 2a^{\alpha\beta} a^{\gamma\delta} . \quad (90)$$

A.5 Linearization of $\mathbf{n} da$

The surface normal \mathbf{n} appears together with the area element da and it is convenient to linearize them together. According to Eqs. (6) and (20) we have

$$\mathbf{n} da = \mathbf{a}_1 \times \mathbf{a}_2 d\Box . \quad (91)$$

Hence

$$\Delta(\mathbf{n} da) = \sum_I \left(N_{I,1} \Delta \mathbf{x}_I \times \mathbf{a}_2 + \mathbf{a}_1 \times N_{I,2} \Delta \mathbf{x}_I \right) d\Box . \quad (92)$$

Expanding $\Delta \mathbf{x}_I$ into $\Delta \mathbf{x}_I = \Delta x_I^\alpha \mathbf{a}_\alpha + \Delta x_I^\eta \mathbf{n}$ we find

$$\begin{aligned} \Delta \mathbf{x}_I \times \mathbf{a}_2 &= J_a (\mathbf{n} \Delta x_I^1 - \mathbf{a}^1 \Delta x_I^\eta) = J_a (\mathbf{n} \otimes \mathbf{a}^1 - \mathbf{a}^1 \otimes \mathbf{n}) \Delta \mathbf{x}_I , \\ \mathbf{a}_1 \times \Delta \mathbf{x}_I &= J_a (\mathbf{n} \Delta x_I^2 - \mathbf{a}^2 \Delta x_I^\eta) = J_a (\mathbf{n} \otimes \mathbf{a}^2 - \mathbf{a}^2 \otimes \mathbf{n}) \Delta \mathbf{x}_I , \end{aligned} \quad (93)$$

where $J_a = \sqrt{\det a_{\alpha\beta}} = da/d\Box$. Thus

$$\Delta(\mathbf{n} da) = (\mathbf{n} \otimes \mathbf{a}^\alpha - \mathbf{a}^\alpha \otimes \mathbf{n}) \mathbf{N}_{,\alpha} \Delta \mathbf{x}_e da . \quad (94)$$

A.6 Linearization of $\tau^{\alpha\beta}$

For the solid model according to Eq. (33) we have

$$\Delta \tau^{\alpha\beta} = \mu (2J^{-3} \Delta J a^{\alpha\beta} - J^{-2} \Delta a^{\alpha\beta}) , \quad (95)$$

which can be rewritten into

$$\Delta \tau^{\alpha\beta} = c^{\alpha\beta\gamma\delta} \mathbf{a}_\gamma \cdot \mathbf{N}_{,\delta} \Delta \mathbf{x}_e , \quad (96)$$

with

$$c^{\alpha\beta\gamma\delta} = \mu J^{-2} \left(4a^{\alpha\beta} a^{\gamma\delta} - \frac{1}{a} (e^{\alpha\gamma} e^{\beta\delta} + e^{\alpha\delta} e^{\beta\gamma}) \right). \quad (97)$$

Note that the tensor $[c^{\alpha\beta\gamma\delta}]$, like $[m^{\alpha\beta\gamma\delta}]$, possesses both major and minor symmetries. For the liquid model according to Eq. (34) we have

$$\Delta\tau^{\alpha\beta} = \gamma (\Delta J a^{\alpha\beta} + J \Delta a^{\alpha\beta}), \quad (98)$$

which can also be written in the form (96), where now

$$c^{\alpha\beta\gamma\delta} = \gamma J \left(\frac{1}{a} (e^{\alpha\gamma} e^{\beta\delta} + e^{\alpha\delta} e^{\beta\gamma}) - a^{\alpha\beta} a^{\gamma\delta} \right). \quad (99)$$

B Finite element tangent matrices

B.1 Tangent matrix associated with G_{int}^e

The internal force vector $\mathbf{f}_{\text{int}}^e$, given in Eq. (65), yields

$$\Delta\mathbf{f}_{\text{int}}^e = \int_{\Omega_0^e} \mathbf{N}_{,\alpha}^T \Delta\tau^{\alpha\beta} \mathbf{N}_{,\beta} dA \mathbf{x}_e + \int_{\Omega_0^e} \mathbf{N}_{,\alpha}^T \tau^{\alpha\beta} \mathbf{N}_{,\beta} dA \Delta\mathbf{x}_e. \quad (100)$$

In view of Eq. (96), we can write

$$\Delta\mathbf{f}_{\text{int}}^e = (\mathbf{k}_{\text{mat}}^e + \mathbf{k}_{\text{geo}}^e) \Delta\mathbf{x}_e \quad (101)$$

where we have introduced the material stiffness matrix

$$\mathbf{k}_{\text{mat}}^e = \int_{\Omega_0^e} c^{\alpha\beta\gamma\delta} \mathbf{N}_{,\alpha}^T (\mathbf{a}_\beta \otimes \mathbf{a}_\gamma) \mathbf{N}_{,\delta} dA \quad (102)$$

and the geometric stiffness matrix

$$\mathbf{k}_{\text{geo}}^e = \int_{\Omega_0^e} \mathbf{N}_{,\alpha}^T \tau^{\alpha\beta} \mathbf{N}_{,\beta} dA \quad (103)$$

Both these matrices are symmetric for the two constitutive models considered here. For those models, the terms in $\mathbf{k}_{\text{mat}}^e$ should be multiplied-out a priori to obtain an efficient implementation. If we consider splitting $\mathbf{f}_{\text{int}}^e$ into $\mathbf{f}_{\text{int}}^e$ and $\mathbf{f}_{\text{int}o}^e$ additional stiffness terms are picked up. These are reported in a forthcoming publication (Sauer, 2013b).

B.2 Tangent matrix associated with G_{ext}^e

From Eq. (69), for dead \mathbf{f}_0 and $\bar{\mathbf{t}}$, we have

$$\Delta\mathbf{f}_{\text{ext}}^e = \int_{\Omega^e} \mathbf{N}^T \mathbf{n} \Delta p da + \int_{\Omega^e} \mathbf{N}^T p \Delta(\mathbf{n} da). \quad (104)$$

The first term is only required for hydrostatic loading according to Eq. (76). Here we find

$$\Delta p = \rho \mathbf{g} \mathbf{N} \Delta\mathbf{x}_e. \quad (105)$$

Contribution $\Delta(\mathbf{n} da)$ is given by Eq. (94). As a result,

$$\mathbf{k}_{\text{ext}}^e = \int_{\Omega^e} \rho \mathbf{N}^T \mathbf{n} \otimes \mathbf{g} \mathbf{N} da + \int_{\Omega^e} p \mathbf{N}^T (\mathbf{n} \otimes \mathbf{a}^\alpha - \mathbf{a}^\alpha \otimes \mathbf{n}) \mathbf{N}_{,\alpha} da. \quad (106)$$

B.3 Tangent contributions associated with the volume constraint

If the volume constraint $g_v = 0$ is active, we need to account for the unknown Lagrange multiplier p_v in the linearization. For the external forces we now have

$$\Delta \mathbf{f}_{\text{ext}}^e = \mathbf{k}_{\text{ext}}^e \Delta \mathbf{x}_e + \mathbf{l}_{\text{ext}}^e \Delta p_v, \quad (107)$$

with

$$\mathbf{l}_{\text{ext}}^e = \frac{\partial \mathbf{f}_{\text{ext}}^e}{\partial p_v} = \int_{\Omega^e} \mathbf{N}^T \mathbf{n} \, da. \quad (108)$$

Further, at the element level,

$$\Delta g_v^e = \mathbf{h}_v^e \Delta \mathbf{x}_e, \quad (109)$$

with

$$\mathbf{h}_v^e = \frac{\partial g_v^e}{\partial \mathbf{x}_e} = -\frac{1}{3} \int_{\Omega^e} \mathbf{n} \cdot \mathbf{N} \, da - \frac{1}{3} \int_{\Omega^e} \mathbf{x} \cdot (\mathbf{n} \otimes \mathbf{a}^\alpha - \mathbf{a}^\alpha \otimes \mathbf{n}) \mathbf{N}_{,\alpha} \, da. \quad (110)$$

The preceding contributions can be arranged into the elemental tangent matrix

$$\mathbf{k}^e := \begin{bmatrix} \mathbf{k}_{\text{int}}^e - \mathbf{k}_{\text{ext}}^e & -\mathbf{l}_{\text{ext}}^e \\ \mathbf{h}_v^e & 0 \end{bmatrix}, \quad (111)$$

which describes the change in $\mathbf{f}_{\text{int}} - \mathbf{f}_{\text{ext}}$ and g_v due to changes in position \mathbf{x}_e and pressure p_v .

Acknowledgements

The authors are grateful to the German Research Foundation (DFG) for supporting this research under projects SA1822/3-2, SA1822/5-1 and GSC 111.

References

- Ambroziak, A. and Klosowski, P. (2006). A four-node 3D isoparametric membrane element. *Task Quarterly*, **10**(1):35–47.
- Arciniega, R. A. and Reddy, J. N. (2007). Tensor-based finite element formulation for geometrically nonlinear analysis of shell structures. *Comput. Methods Appl. Mech. Engrg.*, **196**(4-6):1048–1073.
- Benson, D. J., Bazilevs, Y., Hsu, M.-C., and Hughes, T. J. R. (2011). A large deformation, rotation-free, isogeometric shell. *Comp. Methods Appl. Mech. Engrg.*, **200**(13-16):1367–1378.
- Bischoff, M., Wall, W. A., Bletzinger, K.-U., and Ramm, E. (2004). Models and finite elements for thin-walled structures. In Stein, E., de Borst, R., and Hughes, T. J. R., editors, *Encyclopedia of Computational Mechanics. Vol. 2: Solids and Structures. Chapter 3*. Wiley.
- Bletzinger, K.-U., Wüchner, R., Daoud, F., and Camprubi, N. (2005). Computational methods for form finding and optimization of shells and membranes. *Comput. Meth. Appl. Mech. Engrg.*, **194**(30-33):3438–3452.
- Bonet, J., Wood, R. D., and Mahaney, J. (2000). Aspects of the analysis of membrane structures. In *Computational civil and structural engineering*, pages 105–113. Civil-Comp. Press.

- Borden, M. J., Scott, M. A., Evans, J. A., and Hughes, T. J. R. (2011). Isogeometric finite element data structures based on bezier extraction of NURBS. *Int. J. Numer. Meth. Engng.*, **87**:15–47.
- Brown, R. A., Orr, F. M., and Scriven, L. E. (1980). Static drop on an inclined plate: Analysis by the finite element method. *J. Colloid Interface Sci.*, **73**(1):76–87.
- Bufler, H. (1984). Pressure loaded structures under large deformations. *J. Appl. Math. Mech.*, **64**(7):287–295.
- Contri, P. and Schrefler, B. (1988). A geometrically nonlinear finite element analysis of wrinkled membrane surfaces by a no-compression material model. *Commun. Appl. Numer. M.*, **1**(4):5–15.
- De Lorenzis, L., Temizer, I., Wriggers, P., and Zavarise, G. (2011). A large deformation frictional contact formulation using NURBS-based isogeometric analysis. *Int. J. Numer. Meth. Engng.*, **87**:1278–1300.
- Dong, S. (2012). On imposing dynamic contact-angle boundary conditions for wall-bounded liquid-gas flows. *Comput. Methods Appl. Mech. Engrg.*, **247-248**:179–200.
- Dung, N. T. and Wells, G. N. (2008). Geometrically nonlinear formulation for thin shells without rotation degrees of freedom. *Comput. Methods Appl. Mech. Engrg.*, **197**:2778–2788.
- Flores, F. G. and Estrada, C. F. (2007). A rotation-free thin shell quadrilateral. *Comput. Methods Appl. Mech. Engrg.*, **196**(25-28):2631–2646.
- Fried, I. (1982). Finite element computation of large rubber membrane deformations. *Int. J. Numer. Mech. Engrg.*, **18**:653–660.
- Gosling, P. and Lewis, W. (1996). Optimal structural membranes I. formulation of a curved quadrilateral element for surface definition. *Comput. Struct.*, **61**(5):885–895.
- Gurtin, M. E. and Murdoch, I. (1975). A continuum theory of elastic material surfaces. *Arch. Rat. Mech. Anal.*, **57**(4):291–323.
- Haseganu, E. M. and Steigmann, D. J. (1994). Analysis of partly wrinkled membranes by the method of dynamic relaxation. *Comput. Mech.*, **14**(6):596–614.
- Ibrahimbegovic, A. and Gruttmann, F. (1993). A consistent finite element formulation of nonlinear membrane shell theory with particular reference to elastic rubberlike material. *Finite Elem. Anal. Des.*, **13**(1):75–86.
- Javili, A. and Steinmann, P. (2010). A finite element framework for continua with boundary energies. Part II: The three-dimensional case. *Comput. Meth. Appl. Mech. Engrg.*, **199**:755–765.
- Kiendl, J., Bazilevs, Y., Hsu, M.-C., Wüchner, R., and Bletzinger, K.-U. (2010). The bending strip method for isogeometric analysis of kirchhoff-love shell structures comprised of multiple patches. *Comput. Methods Appl. Mech. Engrg.*, **199**(37-40):2403–2416.
- Kiendl, J., Bletzinger, K.-U., Linhard, J., and Wüchner, R. (2009). Isogeometric shell analysis with kirchhoff-love elements. *Comput. Methods Appl. Mech. Engrg.*, **198**:3902–3914.
- Kloppel, T. and Wall, W. A. (2011). A novel two-layer, coupled finite element approach for modeling the nonlinear elastic and viscoelastic behavior of human erythrocytes. *Biomech. Model. Mechanobiol.*, **10**(4):445–459.

- Kreyszig, E. (1991). *Differential Geometry*. Dover.
- Linhard, J., Wüchner, R., and Bletzinger, K.-U. (2007). "Upgrading" membranes to shells - The CEG rotation free element and its application in structural analysis. *Finite Elem. Anal. Des.*, **44**(1-2):63–74.
- Lu, K., Accorsi, M., and Leonard, J. (2001). Finite element analysis of membrane wrinkling. *Int. J. Numer. Meth. Engng.*, **50**(5):1017–1038.
- Manh, N. D., Evgrafov, A., Gersborg, A. R., and Gravesen, J. (2011). Isogeometric shape optimization of vibrating membranes. *Comp. Meth. Appl. Mech. Engng.*, **200**(13-16):1343–1353.
- Muttin, F. (1996). A finite element for wrinkled curved elastic membranes, and its application to sails. *Comm. Numer. Meth. Engng.*, **12**:775–785.
- Nguyen-Thanh, N., Kiendl, J., Nguyen-Xuan, H., Wüchner, R., Bletzinger, K.-U., Bazilevs, Y., and Rabczuk, T. (2011). Rotation free isogeometric thin shell analysis using pht-splines. *Comput. Methods Appl. Mech. Engng.*, **200**(47-48):3410–3424.
- Oden, J. T. (2006). *Finite Elements of Nonlinear Continua*. Dover Edition.
- Oden, J. T. and Sato, T. (1967). Finite strains and displacements of elastic membranes by the finite element method. *Int. J. Solids Struct.*, **3**(4):471–488.
- Roddeman, D., Drukker, J., Oomens, C., and Janssen, J. (1987). The wrinkling of thin membranes: Part II. Numerical analysis. *J. Appl. Mech.*, **54**(4):888.
- Rumpel, T. and Schweizerhof, K. (2003). Volume dependent pressure loading and its influence on the stability of structures. *Int. J. Numer. Meth. Engng.*, **56**:211–238.
- Sauer, R. A. (2011). Enriched contact finite elements for stable peeling computations. *Int. J. Numer. Meth. Engng.*, **87**:593–616.
- Sauer, R. A. (2013). Local finite element enrichment strategies for 2D contact computations and a corresponding postprocessing scheme. *Comput. Mech.*, **52**(2):301–319.
- Sauer, R. A. (2014). Stabilized finite element formulations for liquid membranes and their application to droplet contact. *Int. J. Numer. Meth. Fluids*, accepted.
- Sauer, R. A. and De Lorenzis, L. (2013). A computational contact formulation based on surface potentials. *Comput. Methods Appl. Mech. Engng.*, **253**:369–395.
- Sauer, R. A. and Holl, M. (2013). A detailed 3D finite element analysis of the peeling behavior of a gecko spatula. *Comp. Meth. Biomech. Biomed. Engng.*, **16**(6):577–591.
- Schweizerhof, K. and Ramm, E. (1984). Displacement dependent pressure loads in nonlinear finite element analyses. *Comput. Struct.*, **18**(6):1099–1114.
- Scott, M. A., Borden, M. J., Verhoosel, C. V., Sederberg, T. W., and Hughes, T. J. R. (2011). Isogeometric finite element data structures based on Bézier extraction of T-splines. *Int. J. Numer. Meth. Engng.*, **88**(2):126–156.
- Simo, J. C. and Fox, D. D. (1989). On a stress resultant geometrically exact shell model. Part I: Formulation and optimal parameterization. *Comput. Meth. Appl. Mech. Engng.*, **72**:267–304.

- Simo, J. C., Fox, D. D., and Rifai, M. S. (1990). On a stress resultant geometrically exact shell model. Part III: Computational aspects of the nonlinear theory. *Comput. Meth. Appl. Mech. Engrg.*, **79**:21–70.
- Stanuszek, M. (2003). FE analysis of large deformations of membranes with wrinkling. *Finite. Elem. Anal. Des.*, **39**(7):599–618.
- Steigmann, D. J. (1999). On the relationship between the Cosserat and Kirchhoff-Love theories of elastic shells. *Math. Mech. Solids*, **4**:275–288.
- Tang, S. C. (1982). Large strain analysis of an inflating membrane. *Comput. Struct.*, **15**(1):71–78.
- Temizer, I., Wriggers, P., and Hughes, T. J. R. (2012). Three-dimensional mortar-based frictional contact treatment in isogeometric analysis with NURBS. *Comput. Methods Appl. Mech. Engrg.*, **209-212**:115–128.
- Weinberg, K. and Neff, P. (2008). A geometrically exact thin membrane model - investigation of large deformation and wrinkling. *Int. J. Numer. Meth. Engng.*, **74**:871–893.
- Wriggers, P. (2006). *Computational Contact Mechanics*. Springer, 2nd edition.
- Wriggers, P. (2008). *Nonlinear Finite Element Methods*. Springer.
- Wriggers, P. and Taylor, R. L. (1990). A fully non-linear axisymmetrical membrane element for rubber-like materials. *Engrg. Comput.*, **7**(1):303–310.
- Wu, B., Du, X., and Tan, H. (1996). A three-dimensional FE nonlinear analysis of membranes. *Comput Struct.*, **59**(4):1–5.
- Youn, S.-K. and Lee, E.-S. (2006). Finite element analysis of wrinkling membrane structures with large deformations. *Finite Elem. Anal. Des.*, **42**(8-9):780–791.